AD-A116 262 ARIZONA UNIV TUCSON ENGINEERING EXPERIMENT STATION F/G 20/4
TRANSONIC AIRFOILS WITH A GIVEN PRESSURE DISTRIBUTION,(U)
JUN 81 A HASSAN, A R SEEBASS, M SOBIECZKY N00014-76-C-0182
UNCLASSIFIED TFD-81-05 NL

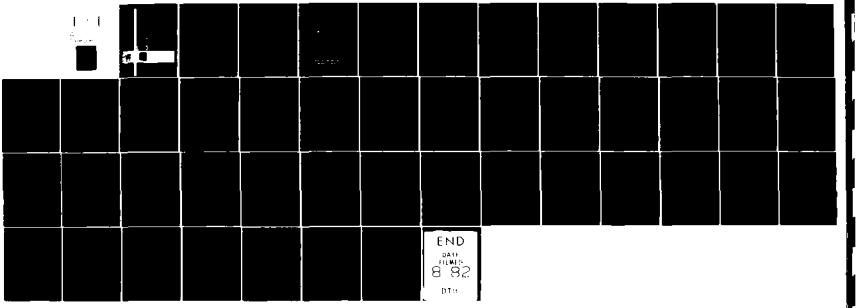

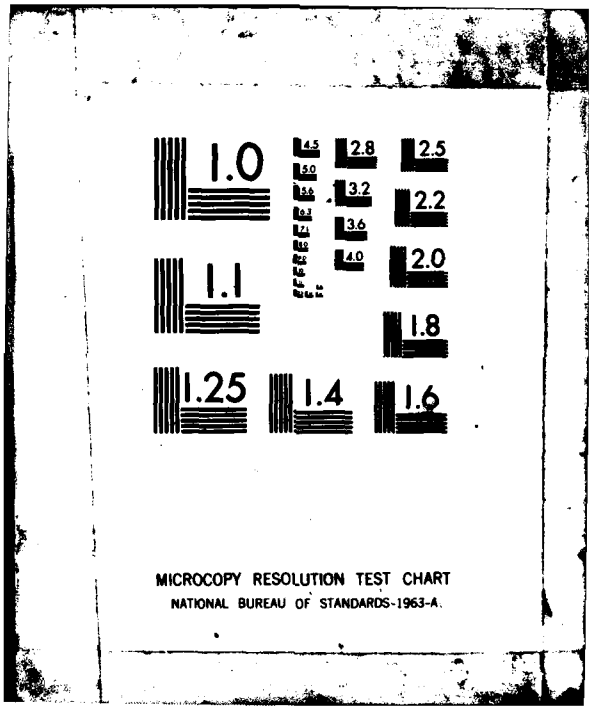
1.0
1.1
1.25
1.4
1.6
1.8
2.0
2.2
2.5
2.8
3.2
3.6
4.0
4.5
5.0
MICROCOPY RESOLUTION TEST CHART
NATIONAL BUREAU OF STANDARDS-1963-A.

TRANSONIC FLUID DYNAMICS

Report TFD 81-05

A. Hassan, A. R. Seebass
H. Sobieczky

TRANSONIC AIRFOILS WITH A GIVEN PRESSURE DISTRIBUTION

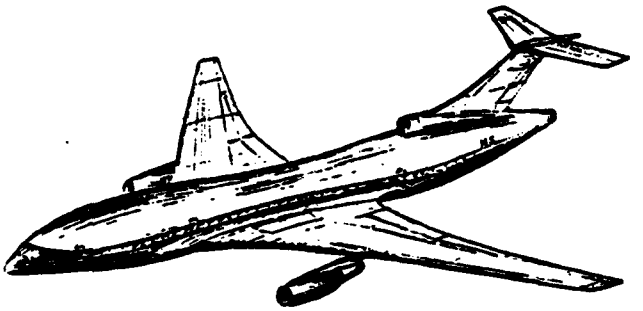

June 1981

Naval Research Laboratory

ENGINEERING EXPERIMENT STATION
COLLEGE OF ENGINEERING
THE UNIVERSITY OF ARIZONA
TUCSON, ARIZONA 85721

SECURITY CLASSIFICATION OF THIS PAGE *(When Data Entered)*

REPORT DOCUMENTATION PAGE	READ INSTRUCTIONS BEFORE COMPLETING FORM
1. REPORT NUMBER	2. GOVT ACCESSION NO. AD-A116 262 / 3. RECIPIENT'S CATALOG NUMBER
4. TITLE *(and Subtitle)* TRANSONIC AIRFOILS WITH A GIVEN PRESSURE DISTRIBUTION	5. TYPE OF REPORT & PERIOD COVERED
	6. PERFORMING ORG. REPORT NUMBER TFD 81-05
7. AUTHOR(s) A. Hassan, A. R. Seebass, and H. Sobieczky	8. CONTRACT OR GRANT NUMBER(s) N00014-76-C-0182
9. PERFORMING ORGANIZATION NAME AND ADDRESS University of Arizona Aerospace and Mechanical Engineering Tucson, Arizona 85720	10. PROGRAM ELEMENT, PROJECT, TASK AREA & WORK UNIT NUMBERS
11. CONTROLLING OFFICE NAME AND ADDRESS Office of Naval Research (code 438) Arlington, Virginia 22217	12. REPORT DATE June 1981
	13. NUMBER OF PAGES 43
14. MONITORING AGENCY NAME & ADDRESS *(if different from Controlling Office)* Office of Naval Research Resident Representative Room 223 Bandelier Hall West University of New Mexico Albuquerque, NM 87131	15. SECURITY CLASS. *(of this report)* Unclassified
	15a. DECLASSIFICATION/DOWNGRADING SCHEDULE

16. DISTRIBUTION STATEMENT *(of this Report)*

Approved for Public Release: distribution unlimited.

17. DISTRIBUTION STATEMENT *(of the abstract entered in Block 20, if different from Report)*

18. SUPPLEMENTARY NOTES

19. KEY WORDS *(Continue on reverse side if necessary and identify by block number)*

Airfoil Design

20. ABSTRACT *(Continue on reverse side if necessary and identify by block number)*

An inverse design procedure for airfoils, based on hodograph techniques, has been developed. For subcritical flows the subsonic portion of the pressure distribution is prescribed; for supercritical flows the stream function on the sonic line is given instead of the supercritical portion of the pressure distribution. In the special variables we use, the equation for the stream function may be solved iteratively using a fast Poisson solver, for the subsonic portion of the flow; for supercritical flows,

DD FORM 1 JAN 73 1473 EDITION OF 1 NOV 65 IS OBSOLETE S/N 0102-014-6601 |

SECURITY CLASSIFICATION OF THIS PAGE *(When Data Entered)*

the supersonic portion is calculated using a characteristic calculation. The results are then mapped back to the physical plane to determine the airfoil shape. Both subcritical and supercritical results are presented. They show good agreement with the direct computation of the flow past the designed airfoil.

AIAA-81-1235 Transonic Airfoils with a Given Pressure Distribution

A. Hassan and A. R. Seebass, University of Arizona, Tucson, AZ; and H. Sobieczky, DFVLR, Gottingen, FRG

AIAA 14th Fluid and Plasma Dynamics Conference

June 23-25, 1981/Palo Alto, California

ABSTRACT

An inverse design procedure for airfoils, based on hodograph techniques, has been developed. For subcritical flows the subsonic portion of the pressure distribution is prescribed; for supercritical flows the stream function on the sonic line is given instead of the supercritical portion of the pressure distribution. In the special variables we use, the equation for the stream function may be solved iteratively using a fast Poisson solver, for the subsonic portion of the flow; for supercritical flows, the supersonic portion is calculated using a characteristic calculation. The results are then mapped back to the physical plane to determine the airfoil shape. Both subcritical and supercritical results are presented. They show good agreement with the direct computation of the flow past the designed airfoil.

INTRODUCTION

In the last decade there has been much interest in transonic aerodynamics. In the case of commercial aircraft this interest stems mainly from the requirement for increased efficiency. This requirement has driven the operating conditions of aircraft compressors, turbines, and propellers, as well as the aircraft themselves, into the transonic regime. Unfortunately once local regions of supersonic flow occur shock waves are likely, with the attendant wave drag and boundary-layer separation losses. A shock-free flow would, of course, be desirable as it avoids these losses. But in the mid 1950s Morawetz[1] showed that shock-free, two-dimensional, irrotational near-sonic flows are mathematically isolated (i.e., any small arbitrary changes in the upstream flow or airfoil shape will lead to the formation of a shock wave). As a consequence, it was felt for some time that shock-free flows could not be achieved in practice. Subsequent wind tunnel research carried out by Pearcey,[2] Whitcomb and Clark[3] and Spee[4] did, however, lead to the development of practical "shock-free" airfoil sections. Parallel with these efforts, shock-free supercritical airfoil flows have been generated in the hodograph plane by Nieuwland,[5] Bauer, Garabedian and Korn,[6] Boerstoel and Huizing,[7] and Sobieczky.[8] More recently, the development of sophisticated numerical codes for the analysis of transonic flow fields has led to the design of both airfoils and wings by numerical optimization (see, e.g., Hicks and Henne[9]).

The design procedure for shock-free supercritical airfoils developed by Garabedian uses the method of complex characteristics and is mathematically elegant. However, even in its user-oriented version[6] practical use of the method is limited to especially trained designers. Nevertheless, some very useful test cases for supercritical airfoils and cascades

were given which have served well as examples for various analysis codes. Another indirect approach was developed by Sobieczky.[8] Here the rheo-electric analogy to the compressible flow equations was used to define a number of transonic airfoil flows. The use of an electric setup, of course, did not provide for economical use of the method, but did lead to a greater understanding of this indirect approach, which had two fruitful consequences: 1) By replacing the electric analog by a digital computer using a fast elliptic solver, we could use all the experience of the analog method concerning boundary conditions that result in interesting airfoil designs. 2) With the development of numerical algorithms for direct non-linear analysis a new method for direct transonic design was developed.[10] Its underlying "fictitious gas concept" is the physical equivalent of the mathematical formulation of the indirect boundary-value problem. The direct approach has the advantage that it can be used also for three-dimensional wings. A description of these two families of methods applied to airfoils is given in Ref. (11).

The design procedure invoked here is an extension and improvement of method 1 above; it requires less than a minute of CYBER 175 CPU time for a supercritical airfoil, and even less for a subcritical airfoil. While the present method is limited to two-dimensional flow, it does allow the user to specify a desired pressure distribution and achieve it with little difficulty through an iterative process.

FORMULATION

The mathematical formulation of the problem assumes a steady, two-dimensional, irrotational flow of a perfect gas. The basic equations of motion are

$$\underline{\nabla} \cdot \rho\underline{q} = 0, \tag{1}$$

$$\underline{\nabla} \times \underline{q} = 0, \tag{2}$$

and

$$\frac{p}{\rho^{\gamma}} = \text{constant}. \tag{3}$$

We satisfy the first of the equations by introducing the usual stream function

$$\psi_y = \rho u = \rho q \, \text{Cos}(\theta),$$

$$\psi_x = -\rho v = -\rho q \, \text{Sin}(\theta). \tag{4}$$

We satisfy the second by defining a potential function, ϕ, such that

$$\underline{\nabla}\phi = \underline{q}$$

or

$$u = \phi_x, \quad v = \phi_y. \tag{5}$$

Equations (4) and (5) can be combined to give

$$\phi_x = \frac{1}{\rho} \psi_y,$$

$$\phi_y = -\frac{1}{\rho} \phi_x, \tag{6}$$

which can be reduced to a single equation in either ψ or ϕ, viz.,

$$\psi_{xx} + \psi_{yy} = \left(\frac{\rho_x}{\rho}\right) \psi_x + \left(\frac{\rho_y}{\rho}\right) \psi_y,$$

$$\phi_{xx} + \phi_{yy} = -\left(\frac{\rho_x}{\rho}\right) \phi_x - \left(\frac{\rho_y}{\rho}\right) \phi_y, \tag{7}$$

with

$$\rho = \rho(q), \quad q = |\underline{\nabla}\phi|. \tag{8}$$

Equations (7) are elliptic for $M < 1$ (subsonic flow), hyperbolic for $M > 1$ (supersonic flow), and parabolic where $M = 1$ (sonic flow). Figure (1) is a sketch illustrating a shock-free supercritical flow field depicting subsonic and supersonic regions of the flow.

To solve either of equations (7) two boundary conditions must be provided. The first of these represents the behavior of the flow in the far field; the second represents the flow tangency condition on the airfoil surface. In the inverse-design procedure under study here, the pressure distribution is used as an input rather than the airfoil coordinates and our goal is to find the shape that an airfoil must have to achieve this input pressure distribution. Accordingly for the inverse problem, neither a Neumann boundary condition for ϕ nor a Dirichlet boundary condition for ψ can be prescribed on the airfoil surface since it is unknown. This is in contrast to direct analysis methods where the airfoil geometry is known prior to computational procedure. The inverse problem of a prescribed pressure on a given airfoil is ill-posed. Here we prescribe a general pressure distribution and find an airfoil that has a pressure distribution like that prescribed.

The Hodograph Transformation

In two-dimensional irrotational flow the nonlinear equations (7) for steady flow can be rendered linear by changing the role of the dependent and independent variables. We introduce the complex velocity

$$u - iv = qe^{-i\theta} \tag{9}$$

with u, v, q and θ being functions of a complex variable

$$z = x + iy. \tag{10}$$

We then have, using equations (6, 9) in differential notation,

$$\begin{aligned} d\phi + i\,\frac{1}{\rho}\,d\psi &= (u - iv)(dx + idy) \\ &= qe^{-i\theta}\,dz \end{aligned} \tag{11}$$

and hence, with q and θ as independent variables, and $\rho = \rho(|\underline{\nabla}\phi|)$ we find

$$\begin{aligned} \left(\frac{\partial z}{\partial \theta}\right)_q &= \frac{e^{i\theta}}{q}\left(\frac{\partial \phi}{\partial \theta} + i\,\frac{1}{\rho}\,\frac{\partial \psi}{\partial \theta}\right), \\ \left(\frac{\partial z}{\partial q}\right)_\theta &= \frac{e^{i\theta}}{q}\left(\frac{\partial \phi}{\partial q} + i\,\frac{1}{\rho}\,\frac{\partial \psi}{\partial q}\right). \end{aligned} \tag{12}$$

Differentiating the first equation of (12) with respect to q and the second with respect to θ and then equating real and imaginary parts, we obtain the hodograph equations, viz.,

$$\begin{aligned} \frac{\partial \phi}{\partial \theta} &= \frac{q}{\rho}\,\frac{\partial \psi}{\partial q}, \\ \frac{\partial \phi}{\partial q} &= -\,\frac{1}{\rho q}\,(1 - M^2)\,\frac{\partial \psi}{\partial \theta}. \end{aligned} \tag{13}$$

It is essential in the present design procedure to introduce the Prandtl-Meyer function, ν, defined by

$$\nu = \int_{q^*}^{q} \sqrt{|1 - M^2|}\,\frac{dq}{q} \tag{14}$$

in place of the velocity q in equations (13), which then take their canonical

form and become

$$\phi_\theta = K(\nu)\ \psi_\nu,$$
$$\phi_\nu = \pm K(\nu)\ \psi_\theta. \tag{15}$$

Here the ± signs refer to supersonic and subsonic conditions respectively and

$$K(\nu) = K[\nu(M)] = [|1 - M^2|]^{1/2}/\rho[q(M)]. \tag{15a}$$

A typical hodograph representation (with ν, θ as independent variables) of the flow field sketched in Figure (1) is depicted in Figure (2a).

The airfoil maps into a closed curve containing the stagnation point S at infinity and the sonic line at points a, b. The analytical structure of ψ near $\nu = 0$ and a smooth curvature of the airfoil at the sonic line require the local structure of the airfoil contour near the θ-axis as sketched in Figure (2b). This weakly singular behavior is of importance in the solution of the boundary-value problem, with ψ given along the elliptic boundary (shaded line in detail of Figure 2). The region of the flow in Figure (1) bounded by the dotted contour and the airfoil represents a region in which every point has a velocity and flow angle equal to that of some other point outside this region, e.g., $q_e = q_f$ and $\theta_e = \theta_f$. Therefore points e and f will correspond to the same point in the hodograph plane, which must be considered as a Riemann surface of two sheets with a branch cut (lines dn, cn) connecting them. The local nature of this flow was studied by Lighthill[12] in his hodograph study of compressible flows around lifting airfoils.

Because the governing equations (15) are linear in the hodograph plane, there is usually no particular difficulty in finding solutions to them, by numerical methods if necessary. However, the presence of the second sheet of the two-sheeted Riemann surface and the apriori unknown location of the

airfoil surface represent major obstacles in solving the governing equations in this plane. From equations (15) it can be shown that the second-order derivatives for both ψ and ϕ either are the Laplacian or the wave operator depending on whether or not the flow is subsonic or supersonic. Thus the equations for the subsonic flow are invariant in form under a conformal transformation.

Subsonic Flow Domain

We proceed by assuming a conformal map of the subsonic portion of the two-sheeted Riemann surface of Figure (2) into the unit circle of Figure (3). (The double-connected infinite domain is mapped into a finite simply connected domain through an exponential mapping followed by a square root mapping to unfold the Riemann sheets.) Here part of the boundary of the unit circle corresponds to the airfoil surface wetted by subsonic flow; the remaining part corresponds to the sonic line. The segment comprising the sonic line, $\omega_b \leq \omega \leq \omega_a$ is chosen and the Mach number (or pressure) on the subsonic part of the airfoil prescribed. On the sonic line segment the Mach number is of course 1. Because Bernoulli's equation, viz.,

$$\frac{1}{2} q^2 + \int \frac{dp}{\rho} = \text{constant}$$

provides a correspondence between the values of p and the local sound speed, we may formulate the inverse-design problem in terms of either M or p, and our choice of M is only a matter of convenience. A typical choice of M for a subcritical airfoil with a cusped trailing edge is illustrated in Figure (4).

With the Mach number given on the boundary of the unit circle, and with the subsonic portion of the flow inside the circle, we take advantage

of the fact that the mapping to the ξ_0-plane is conformal. Thus, the Prandtl-Meyer function ν, and the flow deflection angle, θ, are conjugate harmonics, i.e.,

$$F(\xi_0) = \nu + i\theta$$

or

$$\nabla^2\nu(\xi_0) = 0, \tag{16}$$

$$\nabla^2\theta(\xi_0) = 0. \tag{17}$$

Here $F(\xi_0)$ is the mapping function and $\xi_0 = re^{i\omega}$ with r and ω being the radial and angular coordinate measured in the ξ_0-plane. Boundary conditions for equation (16) are provided through the use of equation (14) relating ν and M; that is, knowing the Mach number distribution on the unit circle, we calculate ν employing equation (14). We then solve Laplace's equation for ν inside the unit circle using Fourier series, which accordingly determines the flow deflection angle θ to within a constant. However, the Prandtl-Meyer function ν is logarithmically singular in q($\nu \propto \log(q)$) at the stagnation point, S, which, for convenience, is positioned at $\xi_0 = -1$ in the ξ_0-plane. Therefore, in order to solve the boundary value problem for ν with Fourier series we need first to subtract the logarithmic behavior at point S. This is done as follows:

let $$\bar{F}(\xi_0) = F(\xi_0) - \log(\xi_0 + 1),$$

$$G(\xi_0) = \nu(\xi_0) - \mathrm{Re}\{\log(\xi_0 + 1)\},$$

$$H(\xi_0) = \theta(\xi_0) - \mathrm{Im}\{\log(\xi_0 + 1)\},$$

then equations (16, 17) become

$$\nabla^2 G(\xi_o) = 0, \tag{18}$$

$$\nabla^2 H(\xi_o) = 0. \tag{19}$$

Here Re{....} and Im{....} are the real and imaginary parts of $\log(\xi_o + 1)$ respectively. Equation (18) is then solved inside the unit circle using Fourier series subject to the following boundary condition

$$G(r=1,\omega) = \nu(1,\omega) - \mathrm{Re}\{\log(e^{i\omega} + 1)\}.$$

Having obtained the solution for $G(r,\omega)$ in the unit circle, we then add back the logarithmic singularity to preserve the singular behavior of ν at the stagnation point.

Reformulating the definitions for the partial derivatives in equations (15) in terms of r and ω we obtain

$$\phi_r = -\frac{1}{r} K(\nu)\, \psi_\omega,$$

and (20)

$$\phi_\omega = r\, K(\nu)\, \psi_r.$$

Equations (20) can be reduced to a single equation in either ψ or ϕ. Eliminating ϕ through cross differentiation of equations (20), we find the equation for ψ

$$r^2\psi_{rr} + r\psi_r + \psi_{\omega\omega} = f(M)\{r^2\nu_r\psi_r + \nu_\omega\psi_\omega\}. \tag{21}$$

Here K is a function of M through equation (15a), M is a function of ν through equation (14), and

$$f(M) = -\left(\frac{\gamma + 1}{2}\right)M^4\,(1 - M^2)^{-3/2}. \tag{21a}$$

Equation (21) is the ξ_o-plane counterpart of the physical-plane equation (7) for the stream function. The transformation to hodograph variables ν, θ, followed by a conformal transformation to the ξ_o-plane results in a linear second-order partial differential equation for ψ. In addition to this linearity, the major advantages of these two transformations are the unfolding of the two-sheeted hodograph surface to a single sheet, and the representation of the subsonic portion of an unknown airfoil by a unit circle. But an these advances are not without attendant complexities, albeit minor ones. These difficulties include the presence of point "I" Figure (3) representing the far field inside the unit circle, at which the stream function is singular, and the singularity in f(M) in equation (21a) at M = 1. The first of these minor difficulties is circumvented through a coordinate transformation of the ξ_o-plane into the ξ-plane sketched in Figure (5). The transformation employed is the bilinear transformation which has the form

$$\xi = re^{i\omega} = \left(\frac{A + B\xi_o}{C + D\xi_o}\right) e^{-i\beta}. \tag{22}$$

Here

$$A = \xi_{o_I}(\bar{\xi}_{o_I} - 1),$$

$$B = \bar{\xi}_{o_I}(1 - \xi_{o_I}),$$

$$C = (\bar{\xi}_{o_I} - 1),$$

and

$$D = (1 - \xi_{o_I}).$$

The second difficulty is the singular behavior at f(M) at M = 1, which

implies that $\psi_r \propto \nu^{-1/3}$ on the sonic line. This is circumvented by assuming that the Mach number on the sonic line is slightly less than 1, e.g., $M_{sonic} = 0.995$ and using the local behavior of ψ to extend the results to $M = 1$.

With $\acute{r}$ and $\acute{\omega}$ as new independent variables, the governing equation for ψ becomes

$$\acute{r}^2\psi_{\acute{r}\acute{r}} + \acute{r}\psi_{\acute{r}} + \psi_{\acute{\omega}\acute{\omega}} = f(M)\{\acute{r}^2\nu_{\acute{r}}\psi_{\acute{r}} + \nu_{\acute{\omega}}\psi_{\acute{\omega}}\}. \tag{23}$$

In equation (22) the quantities $\nu_{\acute{r}}$ and $\nu_{\acute{\omega}}$ are evaluated through the utilization of the solution obtained for equation (16) in conjunction with equation (22). That is to say

$$\nu_{\acute{r}} = \frac{1}{\acute{r}} \mathrm{Re}\{\xi\acute{F}(\xi)\},$$

$$\nu_{\acute{\omega}} = -\mathrm{Im}\{\xi\acute{F}(\xi)\},$$

where

$$\acute{F}(\xi) = e^{-i\omega}\left(\nu_r - \frac{i}{r}\nu_\omega\right) \frac{BC + DA}{(B - D\xi_o e^{i\beta})^2} e^{i\beta}.$$

On the portion of the airfoil surface wetted by subsonic flow we have

$$\psi(1,\acute{\omega}) = 0 \qquad \acute{\omega}_a \geq \acute{\omega} \geq \acute{\omega}_b.$$

On the remaining portion of the unit circle, i.e., the sonic line, an arbitrary distribution for the stream function, ψ, is prescribed, viz.,

$$\psi(1,\acute{\omega}) = \psi_s = g(\acute{\omega}) \qquad \acute{\omega}_a \leq \acute{\omega} \leq \acute{\omega}_b$$

The compressible far-field stream function, ψ_∞, is related to its incompressible counterpart, Ψ_∞, via

$$\psi_\infty = \frac{1}{K(\nu_\infty)} \Psi_\infty$$

$$= \frac{1}{K(\nu_\infty)} \mathrm{Im}\{\frac{q_\infty e^{i\alpha}}{(\xi_o - \xi_{o_I})} - \frac{i\Gamma}{2\pi} \log(\xi_o - \xi_{o_I})\}. \qquad (24)$$

Equation (24) is a consequence of the fact that, at point "I" which presents infinity in the ξ_o-plane equations (20) reduce to the familiar Cauchy-Riemann equations (or incompressible flow equations) expressed in polar coordinates. Thus the complex potential defining the far-field stream function is that for an incompressible flow, Ψ_∞, which is related to its compressible counterpart, ψ_∞, via equation (24). Equation (24), in conjunction with equation (22), is then employed in expressing the far-field boundary condition in the ξ-plane.

The boundary value problem for the stream function is now complete, and equation (22) is solved iteratively using a sixth-order accurate fast Poisson solver devised by Roache.[13] The stagnation streamline leaves the contour of an airfoil at a cusped or wedged trailing edge. This defines, in direct analysis, the amount of circulation around the airfoil and the location of the stagnation point near the leading edge. For an indirect method such as the present one, the situation is exactly the reverse: Since the (mapped) stagnation point location is given, we have to vary the circulation until the stagnation streamline reaches the surface exactly at the stagnation point. The mapped location T of the trailing edge results from this adjustment and the trailing edge shape is then cusped: In the computational plane the stagnation streamline leaves the airfoil contour at T at a 90° angle.

The results for the gradients $\psi_{\tilde{r}}$ and $\psi_{\tilde{\omega}}$ along the elliptic boundary consisting of the subsonic portion of the airfoil and the sonic line are

then utilized in finding the inverse-map to the physical plane, equation (11), which can be written as

$$dx(\bar{\omega}) = \frac{1}{q}\{K(\nu)\mathrm{Cos}(\theta)\psi_{\bar{r}} - \frac{1}{\rho}\mathrm{Sin}(\theta)\psi_{\bar{\omega}}\}d\bar{\omega},$$

and (25)

$$dy(\bar{\omega}) = \frac{1}{q}\{K(\nu)\mathrm{Sin}(\theta)\psi_{\bar{r}} + \frac{1}{\rho}\mathrm{Cos}(\theta)\psi_{\bar{\omega}}\}d\bar{\omega}.$$

Equations (25) are numerically integrated along the unit circle starting from the trailing edge T on the airfoil's lower surface moving toward the stagnation point S and finally ending at the trailing edge T on the airfoil's upper surface, i.e.,

$$x = x_0 + \int_{\bar{\omega}_T}^{2\pi+\bar{\omega}_T} dx(\bar{\omega}),$$

(26)

$$y = y_0 + \int_{\bar{\omega}_T}^{2\pi+\bar{\omega}_T} dy(\bar{\omega}).$$

The resulting airfoil configuration is then checked to see if it has a reasonable thickness distribution. If not, then the input design parameters must be altered and the design procedure repeated. When a suitable airfoil configuration is found, the second of equations (20) is then numerically integrated to find the potential distribution along the elliptic boundary, i.e.,

$$\phi(1,\bar{\omega}) = \phi_0(1,\bar{\omega}_T) + \int_{\bar{\omega}_T}^{2\pi+\bar{\omega}_T} K(\nu)\psi_{\bar{r}}\, d\bar{\omega}. \qquad (27)$$

Results obtained from the solution of the subsonic flow equations (20) on the sonic line are then used as initial values for solving the supersonic flow equations (15) in the hodograph plane using the method of characteristics explained below.

Supersonic Flow Domain

It follows from equation (15) for the flow in the embedded supersonic region, where $M > 1$, that both ψ and ϕ satisfy the linear wave equations

$$\psi_{\nu\nu} - \psi_{\theta\theta} = -\frac{1}{K(\nu)}\left[\frac{\partial}{\partial\nu} K(\nu)\right] \psi_{\nu},$$

and

$$\phi_{\nu\nu} - \phi_{\theta\theta} = -K(\nu)\left[\frac{\partial}{\partial\nu}\frac{1}{K(\nu)}\right] \phi_{\nu},$$

which have characteristics of the form

$$\frac{d\nu}{d\theta} = \pm 1. \tag{28}$$

Introducing the characteristics coordinates ξ, η defined by

$$\xi = \nu + \theta,$$
$$\eta = \nu - \theta, \tag{28a}$$

and reformulating the partial derivatives in equation (15) in terms of the new coordinates, we obtain

$$\phi_{\xi} = K(\nu)\, \psi_{\xi},$$
and
$$\phi_{\eta} = -K(\nu)\, \psi_{\eta}. \tag{29}$$

Equations (29) may also be expressed as

$$\text{on } \xi = \text{constant} \qquad d\phi + K(\nu)d\psi = 0,$$

$$\text{and} \qquad (30)$$

$$\text{on } \eta = \text{constant} \qquad d\phi - K(\nu)d\psi = 0.$$

With the stream functions $\psi_s(\theta)$ and the potential $\phi_s(\theta)$ data known on the sonic line with coordinates $x_s(\theta)$ and $y_s(\theta)$, we proceed to solve the compatability equations (30) holding along the two families of characteristics using a step-by-step numerical scheme (Massau finite difference scheme). The basic concept of this scheme is the following:

Through each point A,B,C,D,E,F, of the sonic line (line AF in Figure (6)) two Mach lines pass, one of the first family, η = constant (a_1, b_1, c_1, ...f_1), and one of the second family, ξ = constant (a_2, b_2, c_2,...f_2). Since the flow properties at the points of the line AF are known, the constants of equations (30) for each characteristic line $a_1...f_1$, $a_2...f_2$, at each point of AF, are also known. Consequently, equations (30) applied along two characteristics of opposite families, e.g., b_1 and a_2 of Figure (6), give two equations relating ϕ_G to ψ_G. These can be solved to obtain ϕ and ψ at point G as functions of ϕ and ψ at the points A and B, viz.,

$$\psi_G = \frac{1}{2}(\psi_A + \psi_B) + \frac{1}{2K(\nu)}(\phi_A - \phi_B),$$

$$\phi_G = \frac{1}{2}(\phi_A + \phi_B) + \frac{K(\nu)}{2}(\psi_A - \psi_B). \qquad (31)$$

In (31), if we think of ν as a specified function of ξ and η on a rectangular grid, the coefficient $K(\nu)$ may be approximated by average values such that the numerical step-by-step scheme becomes second-order accurate in the mesh size, h. The flow deflection angle, θ, and the Prandtl-Meyer function, ν, are evaluated at the grid nodes using (28a).

Having solved for the flow properties at all grid nodes, we then proceed to search for points of zero stream line values as they represent points on the airfoil upper surface.

The inverse transformation from the hodograph plane to the physical plane is given by equation (11), which we can write at every grid point as

$$dx = \frac{\mathrm{Cos}(\theta)}{q}\, d\phi - \frac{\mathrm{Sin}(\theta)}{\rho q}\, d\psi,$$

$$dy = \frac{\mathrm{Sin}(\theta)}{q}\, d\phi + \frac{\mathrm{Cos}(\theta)}{\rho q}\, d\psi. \tag{32}$$

The Jacobian of transformation is

$$J = \frac{\partial(x,y)}{\partial(\nu,\theta)} = \frac{\partial(\phi,\psi)}{\partial(\nu,\theta)} \left[\frac{\partial(\phi,\psi)}{\partial(x,y)}\right]^{-1}$$

$$= \frac{1}{\rho q^2} (\phi_\nu \psi_\theta - \phi_\theta \psi_\nu). \tag{33}$$

Utilizing equations (15), we find that for supersonic flow

$$J = \frac{K(\nu)}{\rho q^2} (\psi_\theta^2 - \psi_\nu^2)$$

which indicates the possibility of a vanishing Jacobian whenever $|\psi_\theta| = |\psi_\nu|$. It can be easily shown that this condition is satisfied whenever a ψ = constant line is tangent to the characteristics in the hodograph ν-θ plane, i.e., whenever

$$\psi_\eta = 0$$

or

$$\psi_\xi = 0.$$

The locus of points in the hodograph plane for which $J = 0$ is known as a limit line. In the physical plane the image of such a line is a cusped

curve along which the physical surface can be thought to be folded upon itself. Such limit lines indicate the inconsistency of the sonic line data with shock-free flow. Thus, they are only acceptable if they occur below the airfoil's upper surface. However, if they occur above or on the airfoil's upper surface, the sonic line data must be altered by adjusting the input subcritical pressure or the sonic line stream function distributions or both, and the design procedure repeated.

The Use of the Computer Program Package

The computer program package consists of sixteen FORTRAN IV subroutines performing calculations and data transfer. The package makes use of two permanent files for results to be retained and one file for input data.

For a specific airfoil design the program has to be operated in the following manner:

a -- Using the input Mach number and, for supercritical airfoils, the sonic line stream function distributions, both of which must be reasonable, in addition to the two design parameters M_∞ and α, we obtain a subsonic boundary configuration and have it displayed on a computer terminal with graphic capabilities.

b -- The level of the input Mach number distribution on the lower surface ($0 \leq \omega \leq \pi$) is moved slightly in order to shift the location of the far-field singularity in the computational plane. This in turn is sufficient to reduce the x-gap of the trailing edge of the resulting configuration to a preset value (e.g., 10^{-3}).

c -- The input Mach number distribution is then altered in the vicinity of the stagnation point of the resulting configuration to reduce the y-gap at that point.

d -- Once an acceptable subsonic boundary configuration (displayed on the terminal) is obtained the supersonic flow field computation is then carried on to determine the airfoil coordinates under the sonic line. If a limit line is encountered in the supersonic flow domain, steps a through d are repeated for modified input Mach number and sonic line stream function distributions.

Figure (7) is a flow chart illustrating the design procedure discussed above.

COMPUTATIONAL RESULTS

In this section, a number of numerical computational results are presented, and some experience with the algorithm is discussed. A few examples of airfoil designs are presented in Figures (8) through (20). The airfoils cover a range of free-stream Mach numbers and lift coefficients. A comparison with results obtained from the direct computation of the flow field utilizing the designed airfoil geometry as input is also illustrated in Figures (16) and (20) for a subcritical and a supercritical airfoil respectively. The analysis code, FL06, devised by Jameson[14] utilizes a finite-difference method to solve the governing equations iteratively after mapping the airfoil into the unit circle.

For the design of subcritical airfoils with cusped trailing edges, Figures (8) through (15) illustrate the different input Mach number distributions required for the design procedure and the resulting airfoil shapes at M_∞ = 0.573, 0.589, and 0.622. Through a study of the above airfoils we have demonstrated that small modifications in the input Mach number distribution near the stagnation point have a substantial influence on the y-gap at the airfoil trailing edge and, hence, on airfoil closure. That is, increasing the slope of the Mach number distribution at the stagnation point results

in an airfoil with a smaller nose radius and consequently a smaller thickness to chord ratio; this ultimately results in a smaller y-gap at the airfoil trailing edge. Experience has shown that in the process of minimizing the y-gap at the trailing edge the level of the input Mach number distribution has to be altered on the lower surface or the upper surface, or both, to maintain the x-gap at a present value, e.g., 10^{-3}.

Figure (16) compares the results obtained from analysis computation of the flow field utilizing the designed airfoil geometry shown in Figure (9) as input. Results obtained from both the design and analysis show good agreement except near the trailing edge.

The input Mach number distribution for a slightly supercritical airfoil with a cusped trailing edge at $M_\infty = 0.642$ is shown in Figure (17). Results obtained from the two stages of the design procedure, i.e., computation of the subsonic boundary configuration and the complete airfoil shape, are illustrated in Figures (18,19). It should be mentioned here that while the y-gap at the trailing edge for subcritical airfoils can be controlled easily, more effort is required in the case of supercritical airfoils. This is due to the representation of the sonic line as part of the subsonic boundary configuration (see Figure (18)).

Figure (20) illustrates a comparison of results obtained from the direct computation of the flow field of a supercritical airfoil with cusped trailing edge at $M_\infty = 0.75$ resulting from the design procedure invoked here with a different solver for the stream function equation. It can be noticed that good agreement is obtained for the subcritical pressures. The slight disagreement between the supercritical pressures that is observed is due to the numerical difficulty in computing the normal derivative of the stream

function along the sonic line; this has a direct effect on the sonic line coordinates and the supercritical pressures.

CONCLUSION

Based on hodograph theory an efficient design procedure has been developed that can be used for the aerodynamic design of subcritical as well as shock-free supercritical airfoil sections. An analysis of the numerical solutions obtained with this design procedure indicates that only one airfoil configuration is obtained for a desired input target pressure and free-stream flow conditions. Experience has also shown that the input Mach number, the free-stream Mach number and the sonic line stream function distribution cannot be prescribed independently of each other if a practical airfoil configuration is sought. Subcritical airfoils with a target pressure distribution and shock-free supercritical airfoils with a target subsonic pressure distribution can be found with modest effort when the algorithm is in the hands of an experienced user.

Within the framework of our design procedure it seems possible that the procedure can be extended further to study a large class of aerodynamically interesting airfoils and their corresponding pressure distributions. Moreover, while the results are given for inviscid flow, the same procedure can be employed, iteratively, with a boundary-layer calculation (utilizing airfoils with an open trailing edge) in order to achieve viscous airfoil designs. For supercritical airfoils, the shock-free pressure field should make the boundary-layer calculation reliable.

From the engineering point of view, the method was found to be sufficiently accurate and flexible providing results at moderate cost. Indeed, less than

a minute of CYBER 175 CPU time is required for supercritical airfoils; even less is required for subcritical airfoils.

ACKNOWLEDGMENT

This research was carried out by the Computational Mechanics Laboratory at the University of Arizona, Department of Aerospace and Mechanical Engineering. The work was supported by AFOSR Grants 76-2954 and 81-0107, and ONR Grant N0001476-C-0182,P0006.

REFERENCES

[1]Morawetz, C. S., "On the Non-Existence of Continuous Transonic Flows Past Profiles, I, II, and III," Communications on Pure and Applied Mathematics, Vols. 9, 10, and 11, 1956, 1957, and 1958, pp. 45-68, 107-131, and 129-144.

[2]Pearcey, H. H., "The Aerodynamic Design of Section Shapes for Swept Wings," Advances in the Aeronautical Sciences, Vol. 3, 1962, pp. 277-322.

[3]Whitcomb, R. T. and Clark, L. R., "An Airfoil Shape for Efficient Flight at Supercritical Mach Numbers," NASA TM X-1109 (Confidential), July 1965.

[4]Spee, B. M., "Investigation on the Transonic Flow Tunnel Airfoils," NLR Technical Report TR-69122U, 1969.

[5]Nieuwland, G. Y., "Transonic Potential Flow Around a Family of Quasi-Elliptic Aerofoil Sections," NLR Technical Report T. 172, 1967.

[6]Bauer, F., Garabedian, P., and Korn, D., Supercritical Wing Sections III, Lecture Notes in Economics and Mathematical Systems, Springer Verlag, New York, 1977.

[7]Boerstoel, J. W. and Huizing, G. H., "Transonic Shock-Free Aerofoil Design by an Analytic Hodograph Method," AIAA Paper 74-539, AIAA 7th Fluid and Plasma Dynamics Conference, Palo Alto, CA, 1974.

[8]Sobieczky, H., "Entwurf überkritisher Profile mit Hilfe der Rheoelectrischen Analogie," DFVLR Report DLR-FB 75-43, 1975.

[9]Hicks, R. and Henne, P. A., "Wing Design by Numerical Optimization," AIAA Aircraft and Systems Technology Meeting, Seattle, WA, 1977.

[10]Sobieczky, H., Yu, N. J., Fung, K.-Y., and Seebass, A. R., "A New Method of Designing Shock-Free Transonic Configurations," AIAA J., Vol. 17, No. 7, pp. 722-729, 1979.

[11]Sobieczky, H., "Related Analytical, Analog, and Numerical Methods in Transonic Airfoil Design," AIAA Paper 79-1556, AIAA 12th Fluid and Plasma Dynamics Conference, Williamsburg, VA, July 1979.

[12]Lighthill, M. J., "On the Hodograph Transformation for High Speed Flow. II, A Flow with Circulation," Quart. J. Mech. and Appl. Math., Vol. 1, pp. 442-450, 1948.

[13]Roache, P. J., "Sixth-Order Accurate Direct Solver for the Poisson and Helmholtz Equations," AIAA J., Vol. 17, No. 5, pp. 524-526, 1978.

[14]Jameson, A., "Iterative Solution of Transonic Flows over Airfoils and Wings, Including Flows at Mach 1," Communications on Pure and Applied Mathematics, Vol. 27, pp. 283-309, 1974.

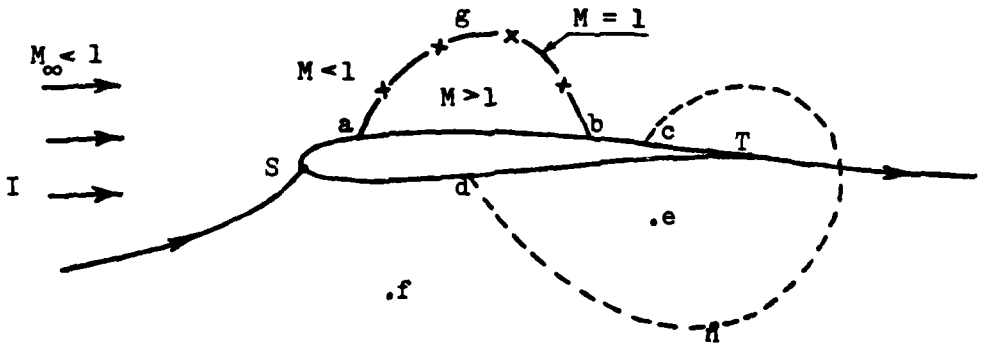

Figure 1. Sketch of shock-free flow past a lifting airfoil (stagnation point S, trailing edge T, far-field I, branch point n).

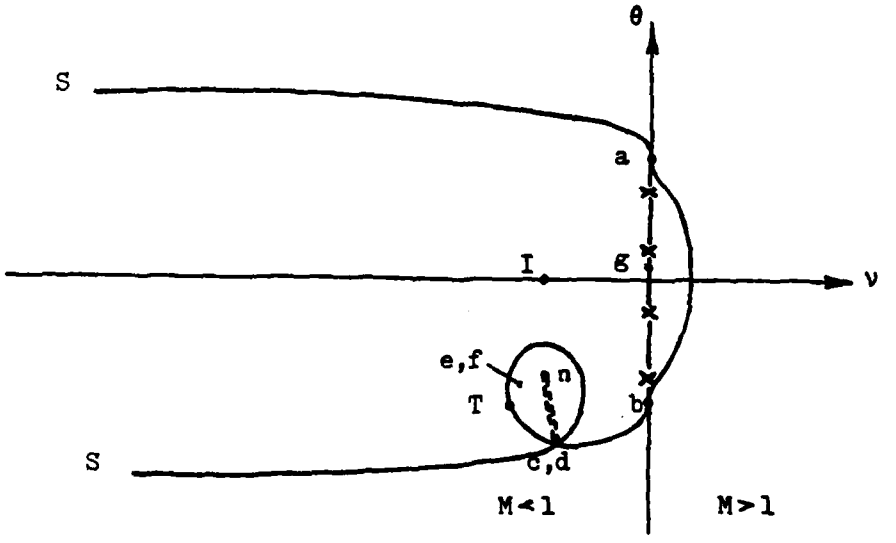

Figure 2a

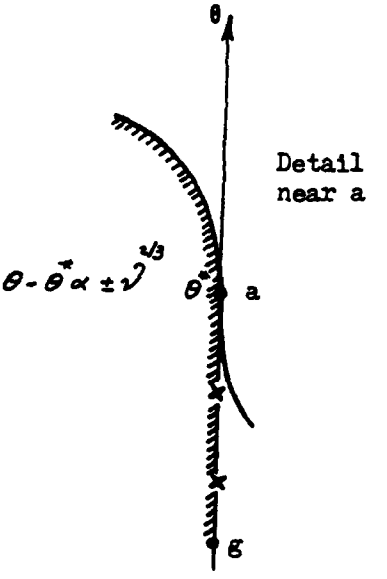

Figure 2b

Figure 2. Hodograph representation of the flow field sketched in figure (1).

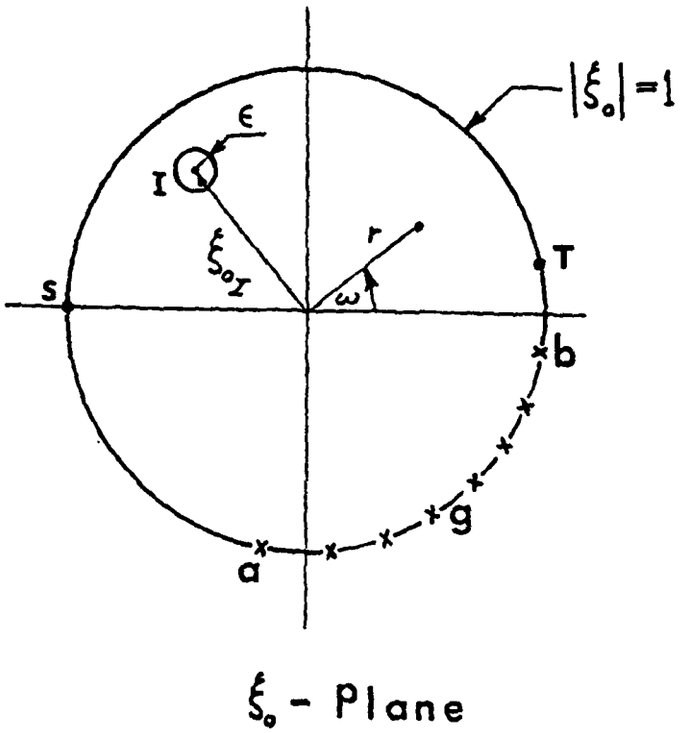

Figure 3. Airfoil subsonic-sonic boundary in the ξ_o-plane (stagnation point S, trailing edge T, far field I).

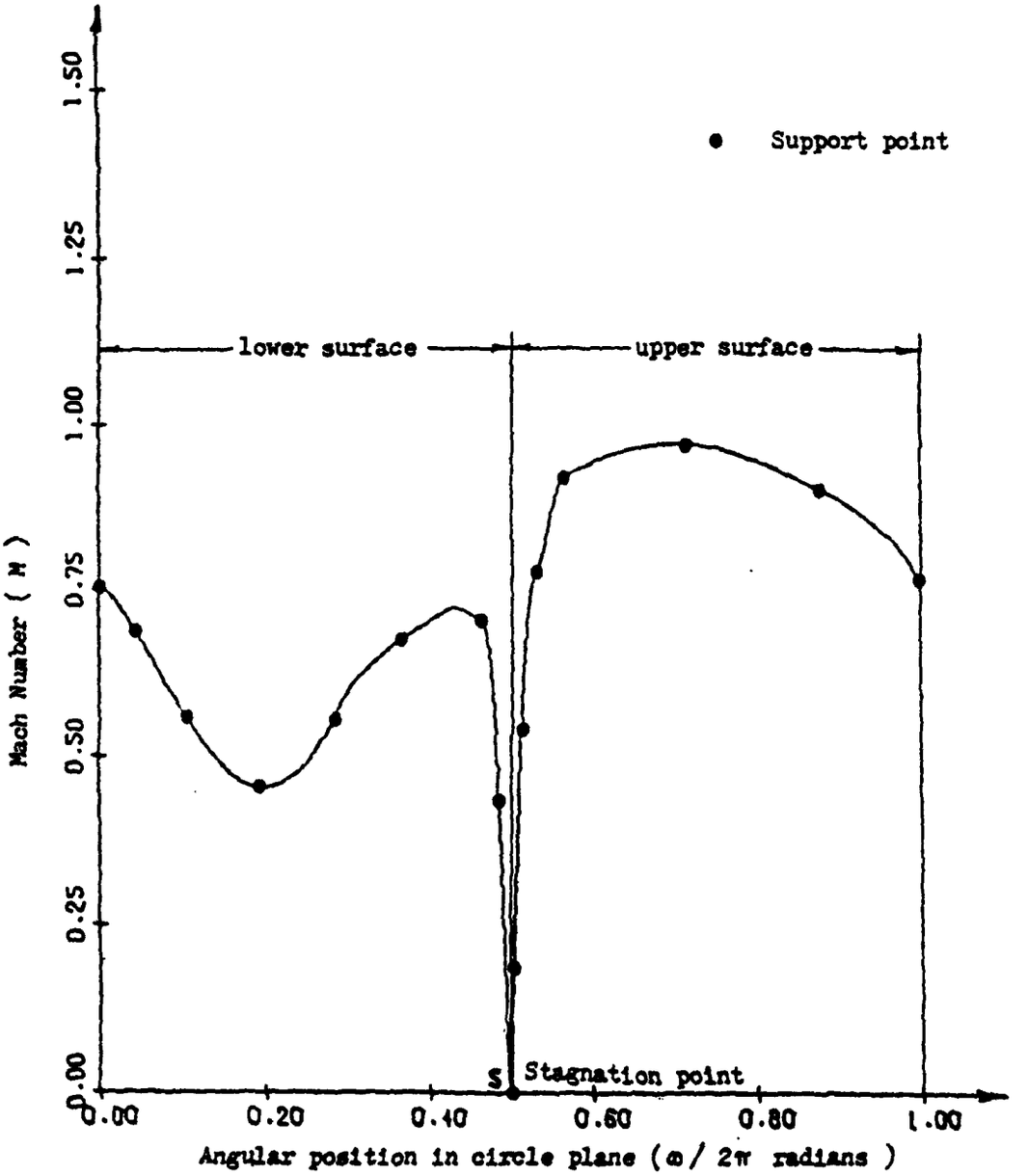

Figure 4. Typical input Mach number distribution. The location of the trailing edge T is not known in advance.

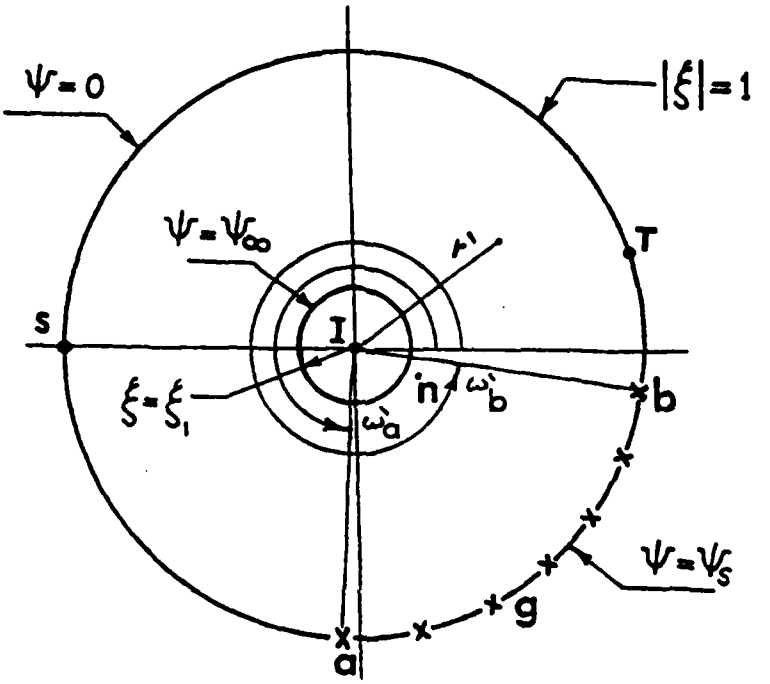

Figure 5. Airfoil subsonic-sonic boundary in the computational plane (stagnation point S, trailing edge T, far field I, branch point n).

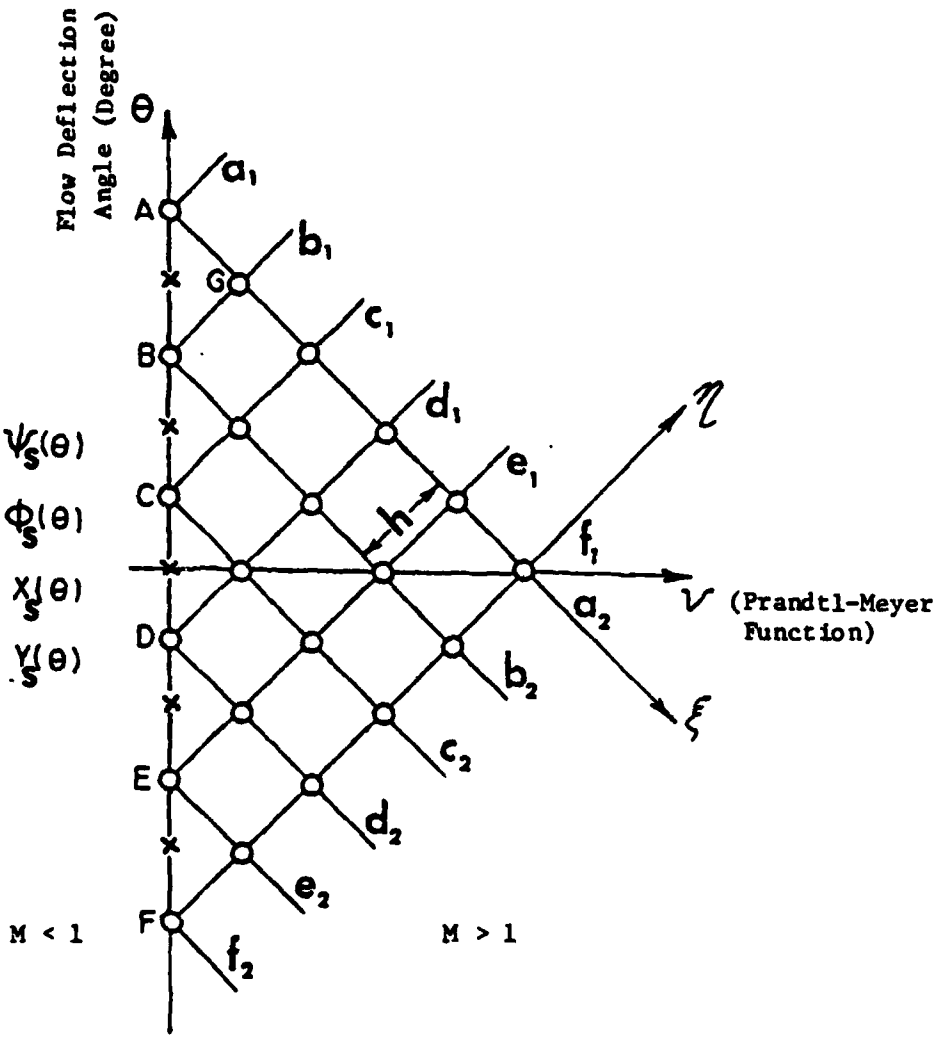

Figure 6. Computation of the supersonic flow field in the hodograph plane (ν-θ) using the method of characteristics.

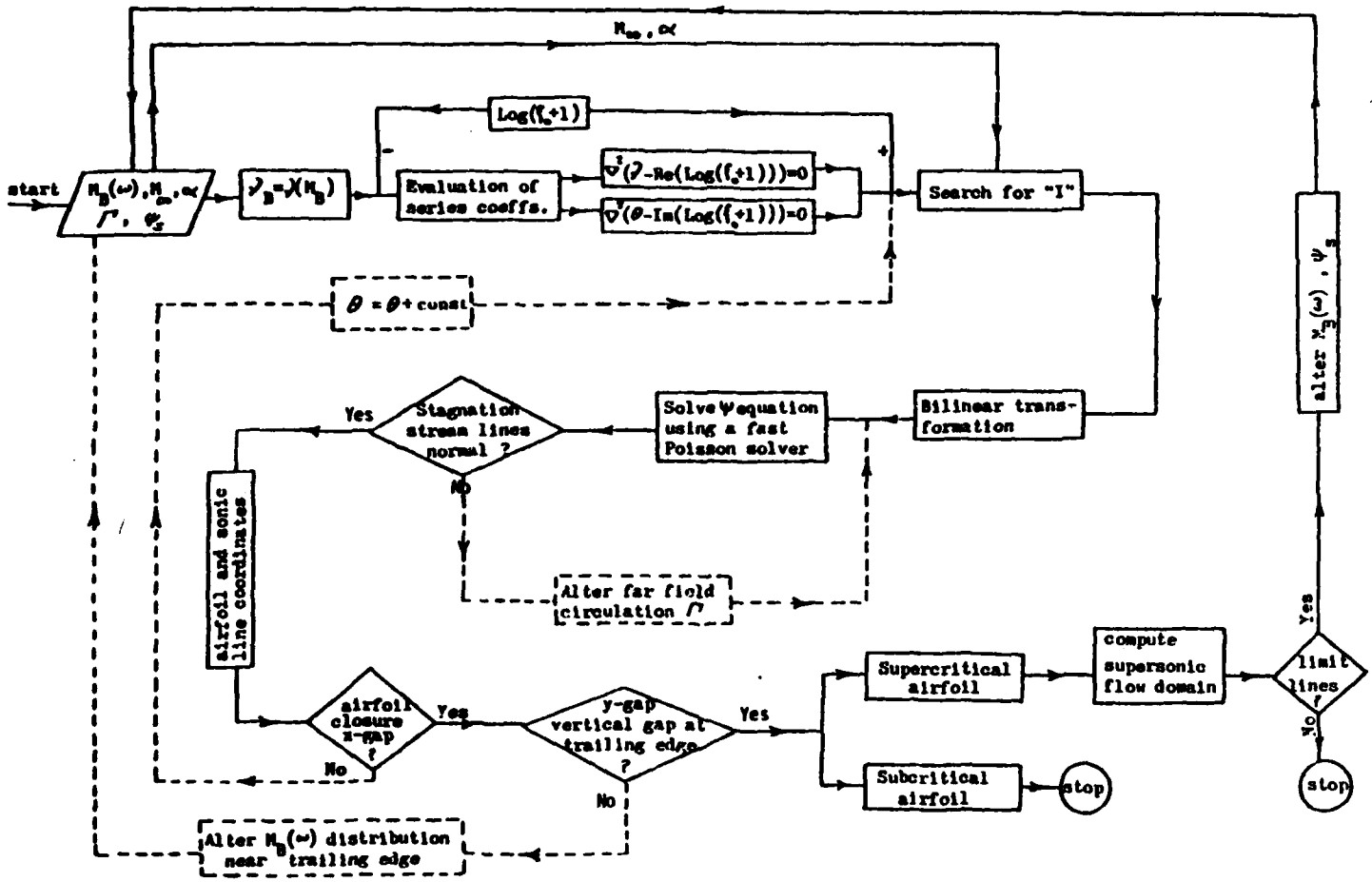

Figure 7. Flow chart indicating the design procedure.

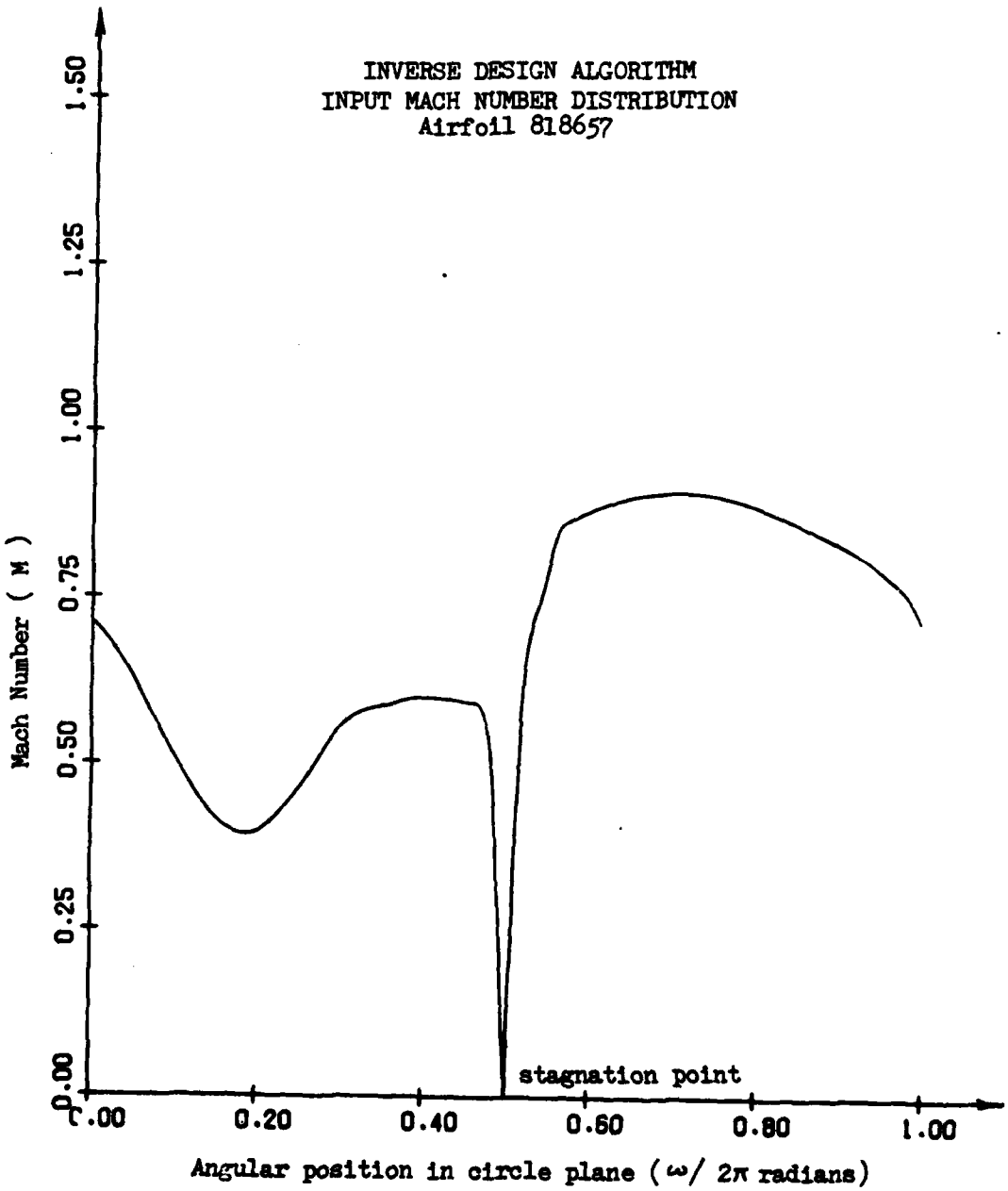

Figure 8. Input Mach number distribution for a sub-critical airfoil with cusped trailing edge at $M_\infty = 0.573$.

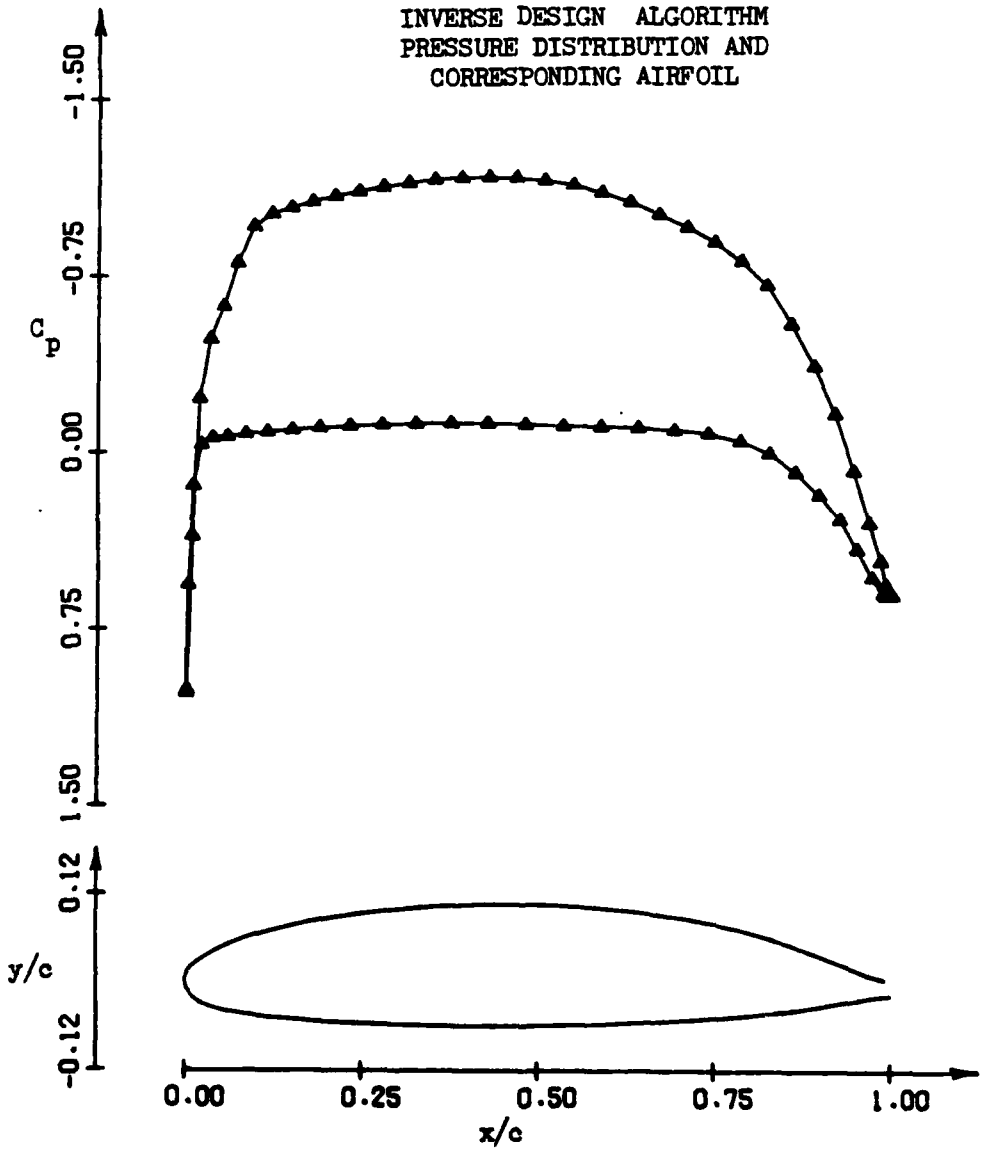

Figure 9. Airfoil 818657

M_∞ =0.5730 C_L =0.6932 C_D =0.0003 A.O.A. = 0.0°

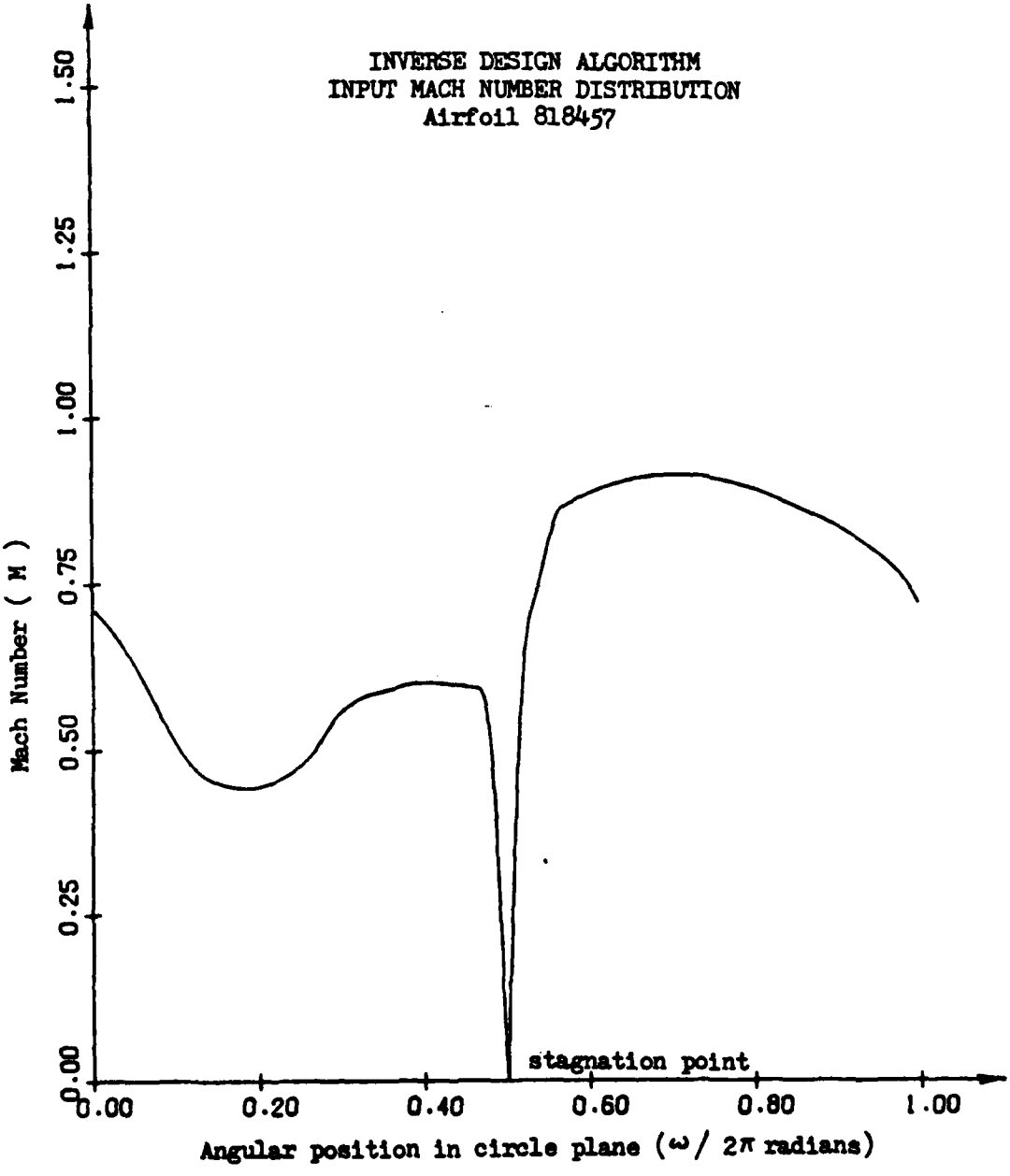

Figure 10. Input Mach number distribution for a subcritical airfoil with cusped trailing edge at $M_\infty = 0.573$.

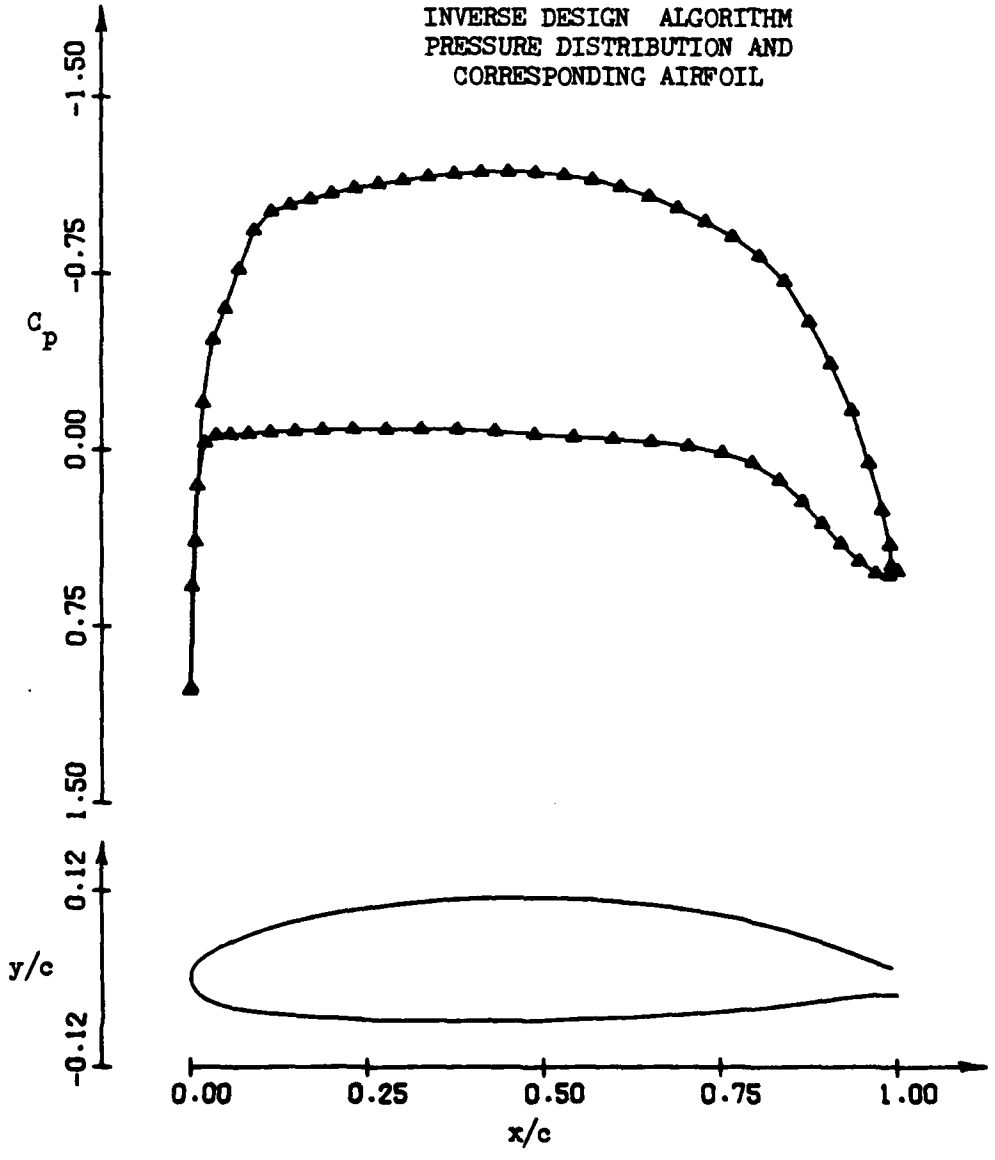

Figure 11. Airfoil 818457

M_∞ =0.5730 C_L =0.6845 C_D =0.0002 A.O.A. =0.0°

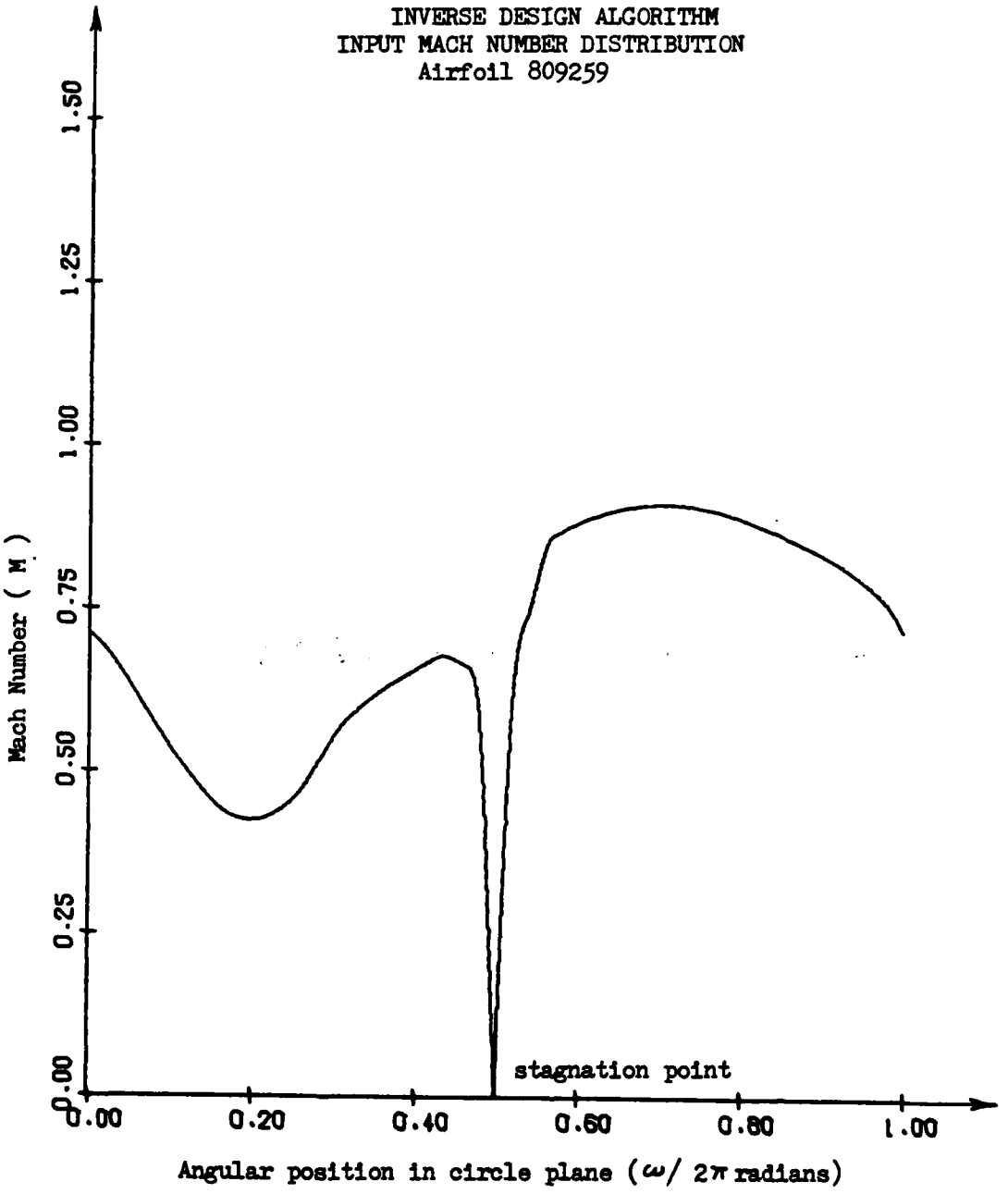

Figure 12. Input Mach number distribution for a subcritical airfoil with cusped trailing edge at M_∞=0.589.

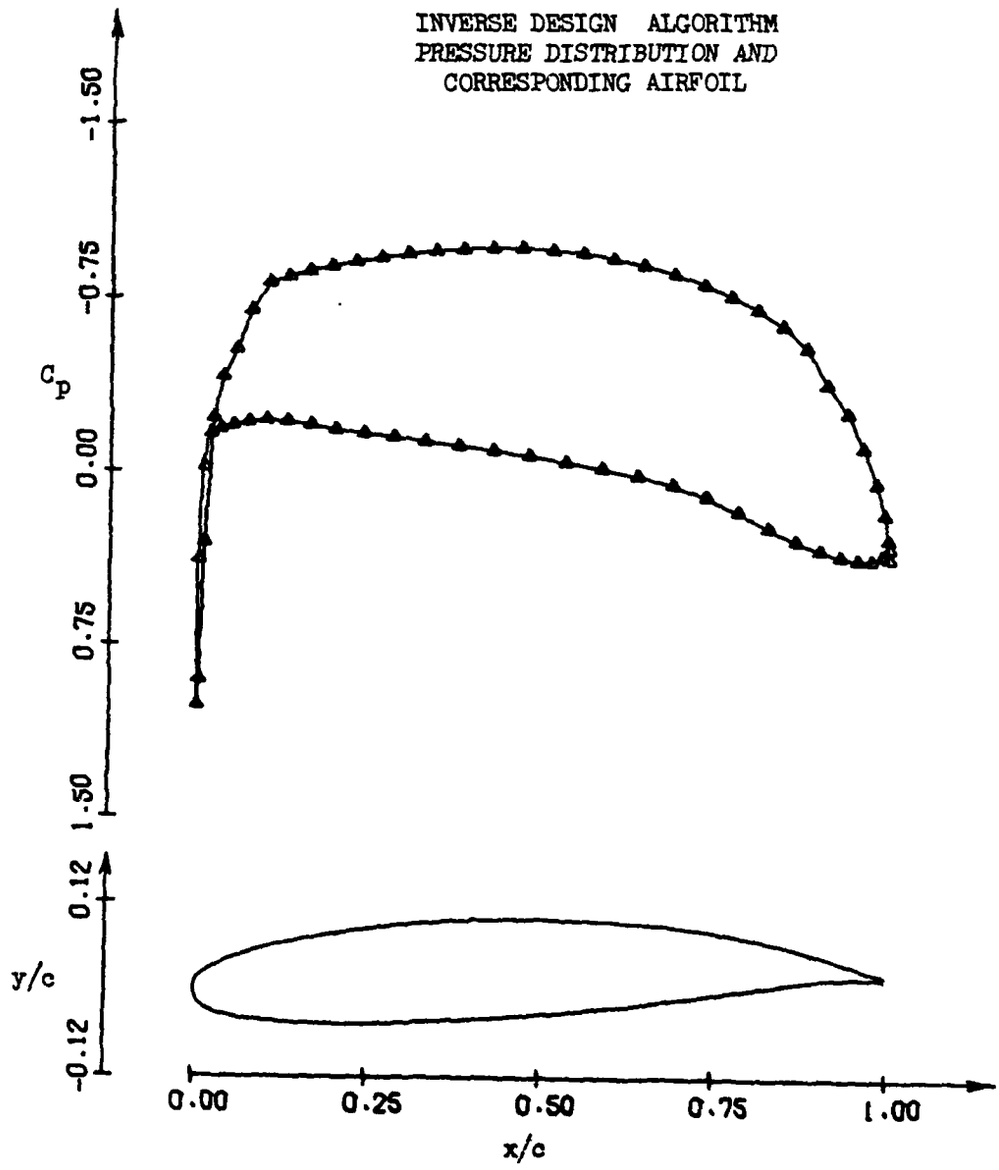

Figure 13. Airfoil 809259

M_∞ =0.589 C_L =0.7493 C_D =0.0001 A.O.A. =1.281°

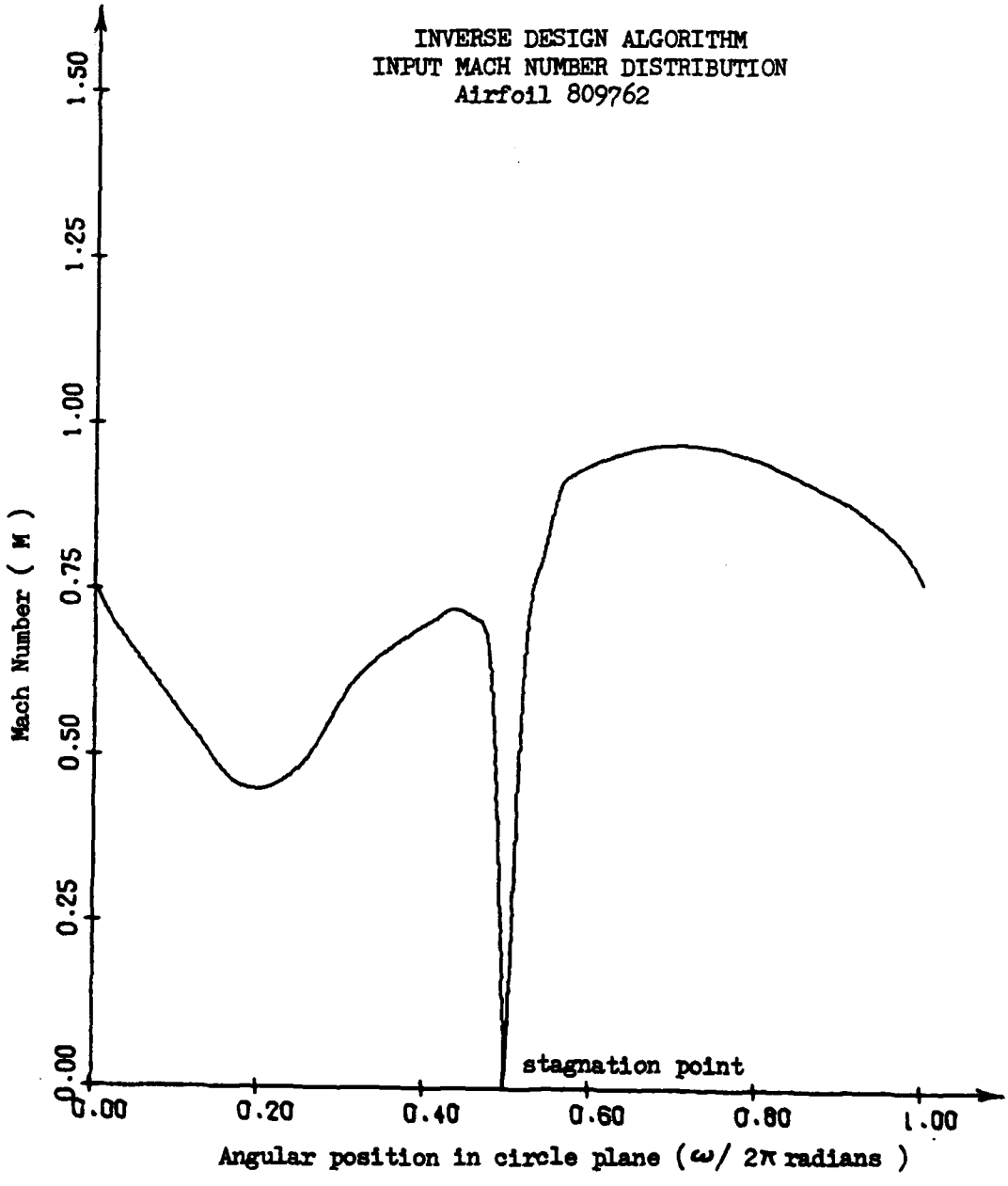

Figure 14. Input Mach number distribution for a sub-critical airfoil with cusped trailing edge at M_∞=0.622.

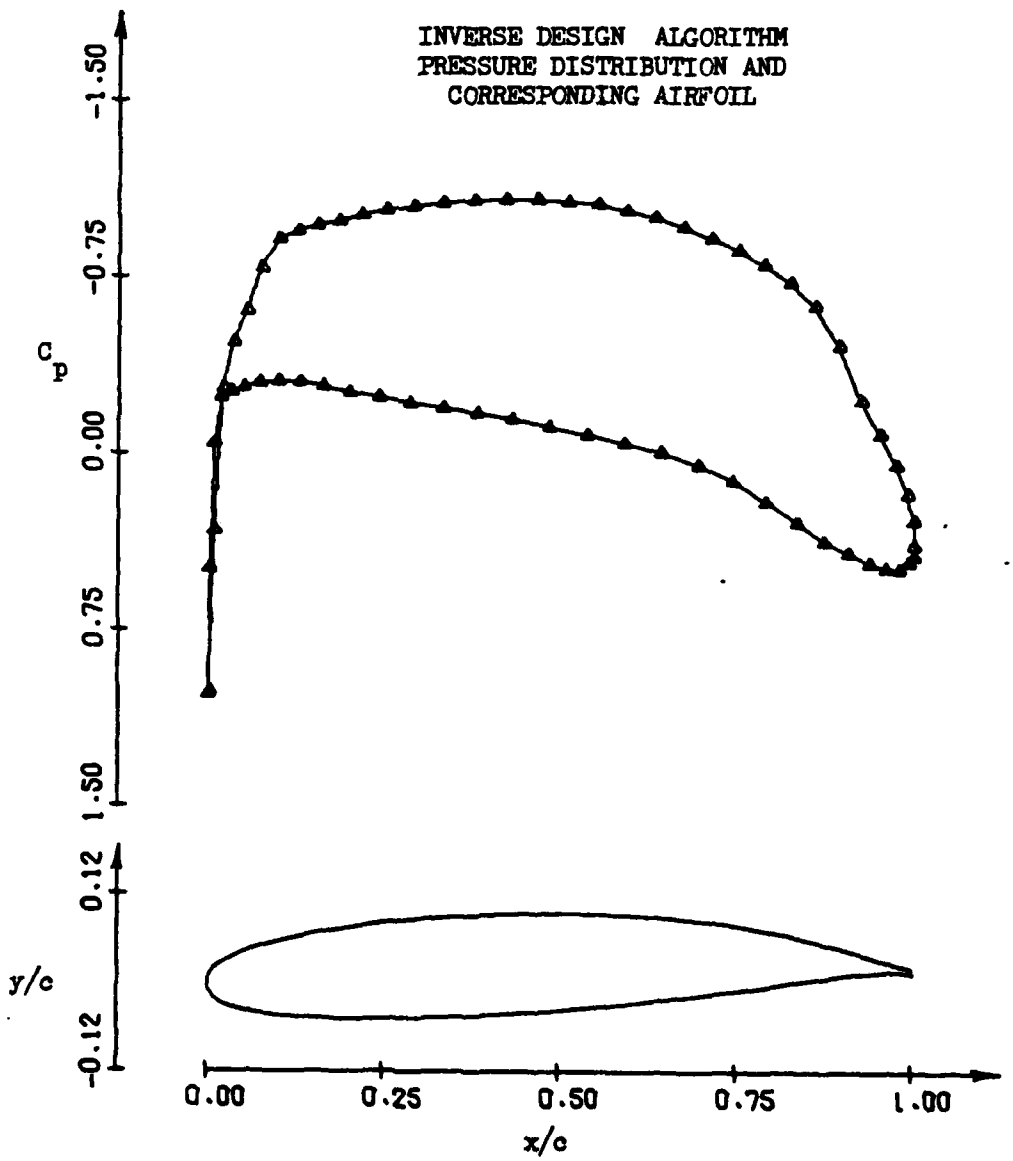

Figure 15. Airfoil 809762

M_∞ =0.622 C_L =0.7984 C_D =0.0001 A.O.A. =1.027°

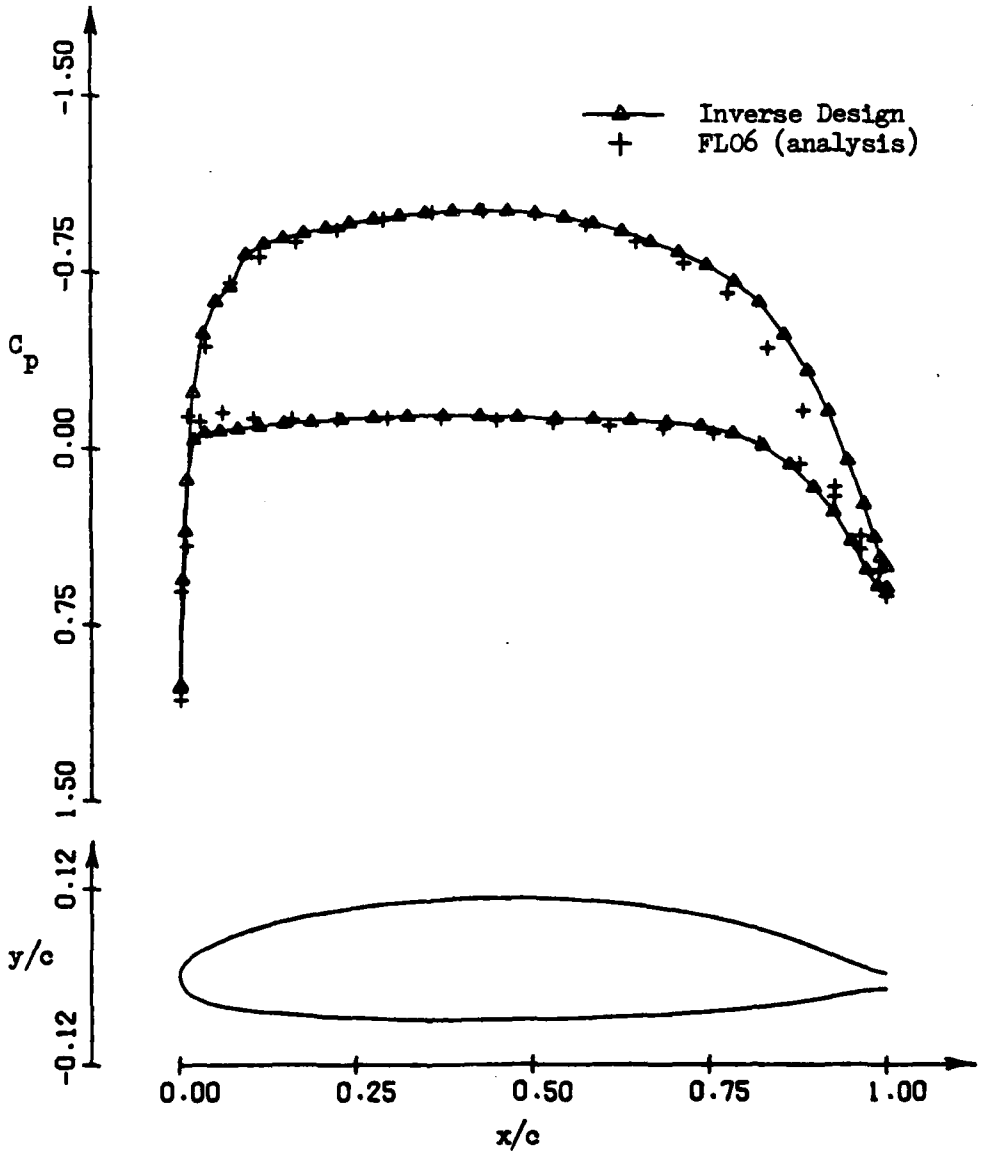

Figure 16. Airfoil 818657

Inverse M_∞ =0.573 C_L =0.6932 C_D =0.0003 A.O.A. =0.00°
F106 M_∞ =0.573 C_L =0.6484 C_D =0.0001 A.O.A. =0.55°

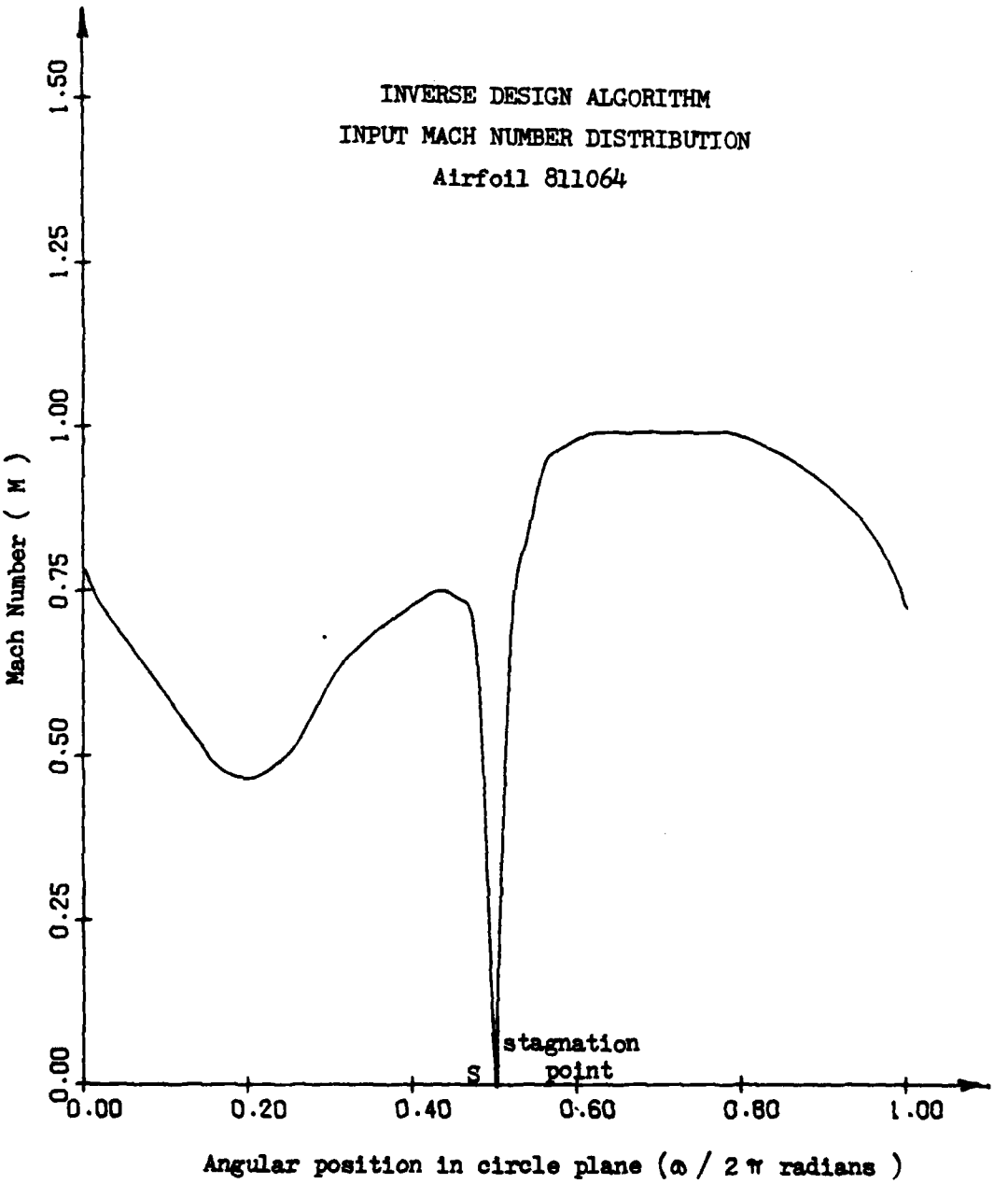

Figure 17. Input Mach number distribution for a supercritical airfoil with cusped trailing edge at M_∞ =0.642.

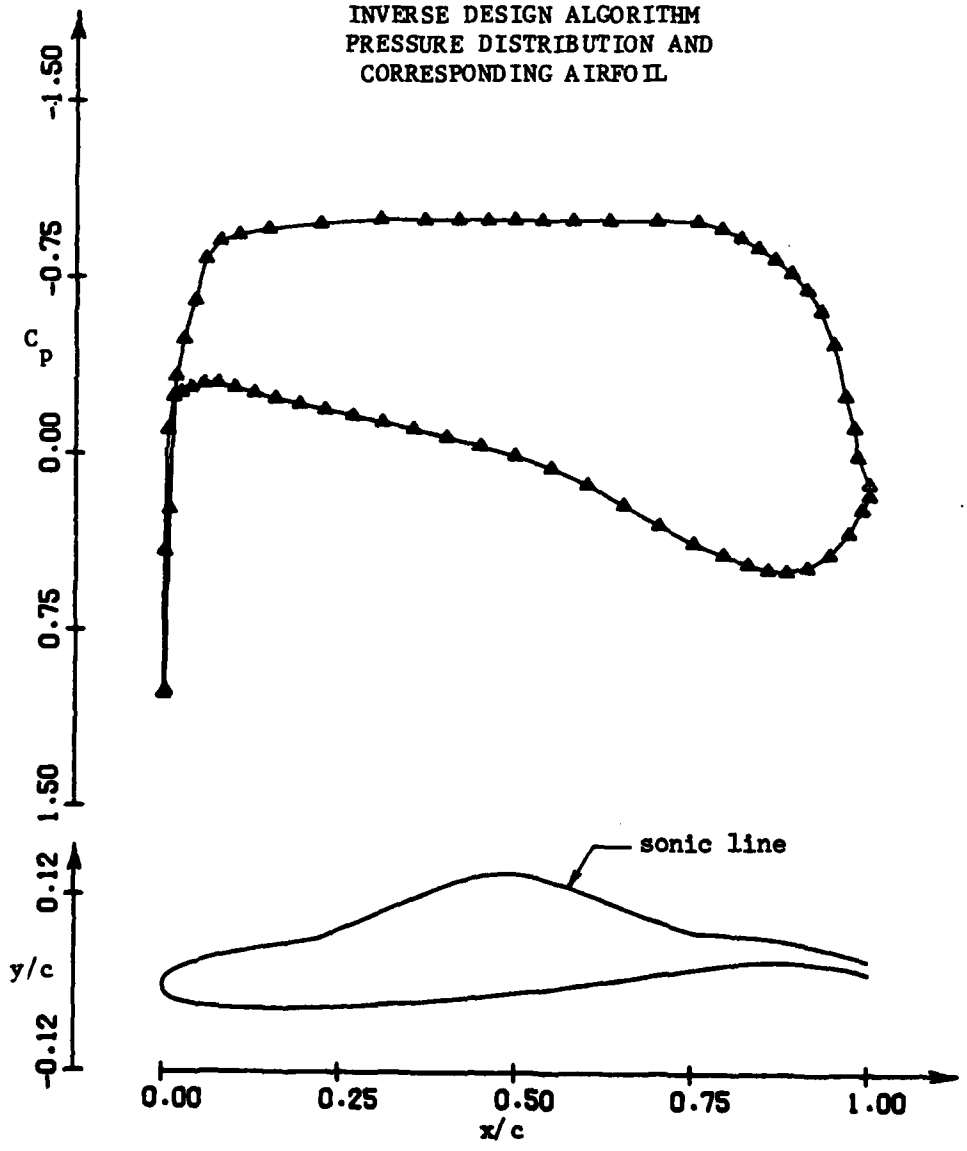

Figure 18. Airfoil 811064

M_∞ = 0.642 C_L = 0.943 C_D = -0.0006 A.O.A. = 1.507°

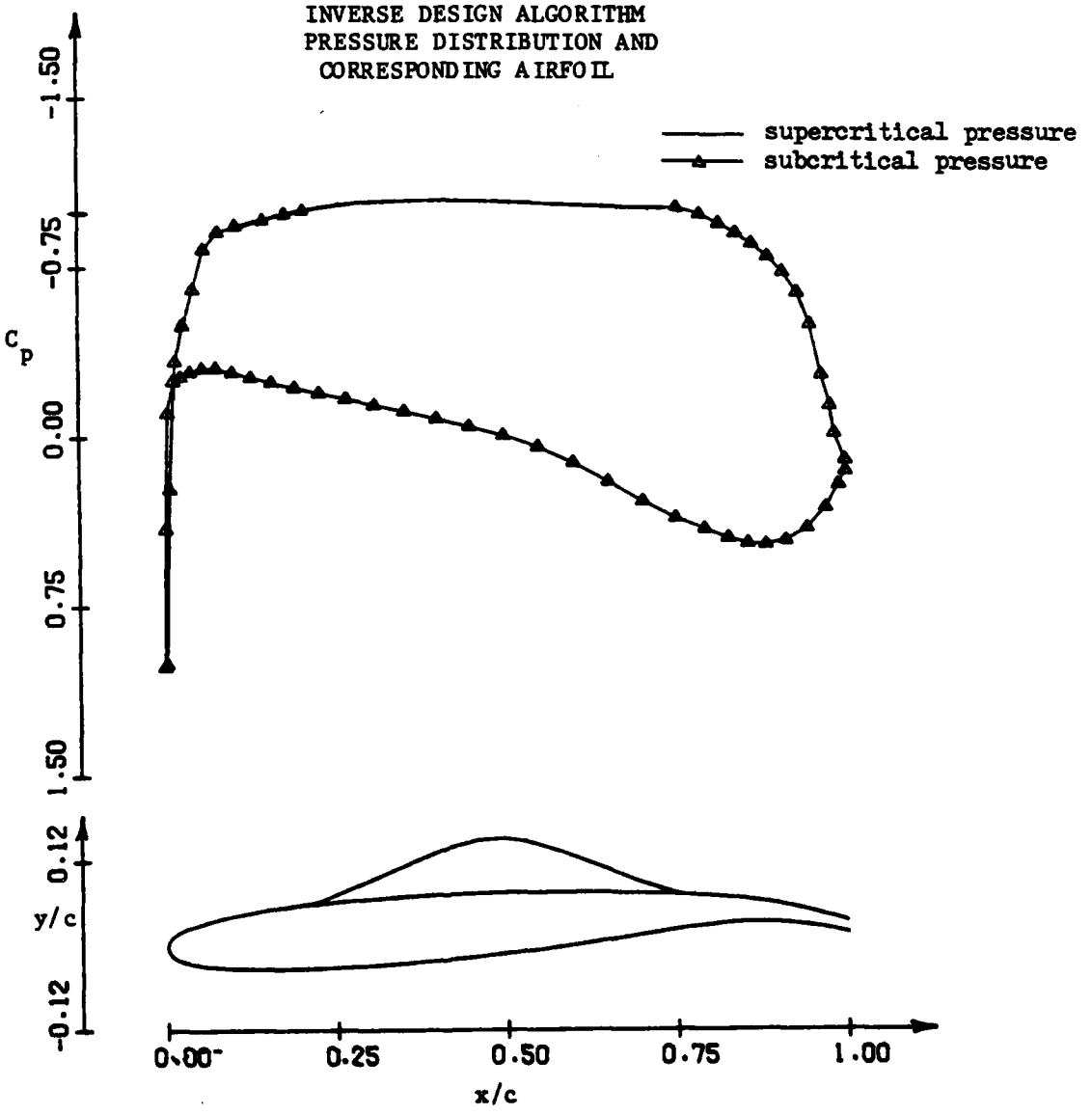

Figure 19. Airfoil 811064

$M_\infty = 0.642$ $C_L = 0.987$ $C_D = -0.0009$ A.O.A. = 1.507°

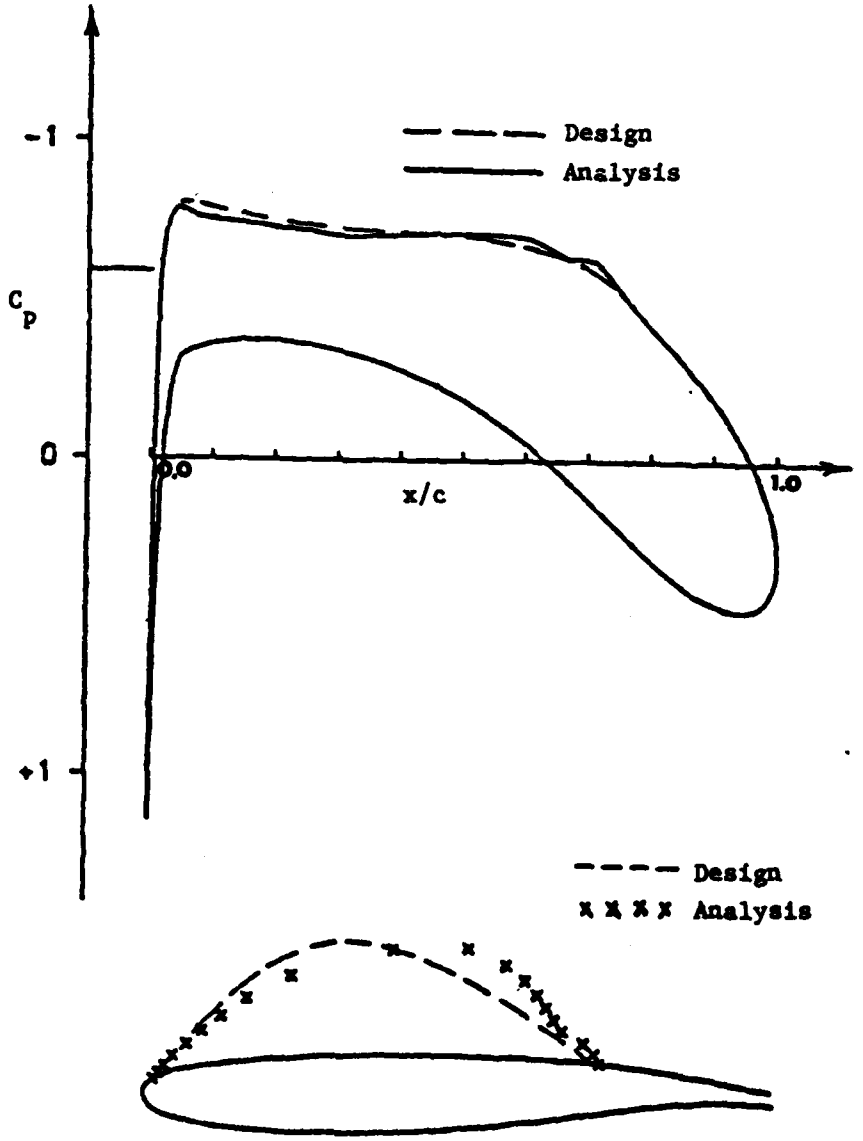

Figure 20. Airfoil 68255

Inverse M_∞ =0.75 C_L =0.53 C_D =0.000 A.O.A =0.0°

FL06 M_∞ =0.75 C_L =0.53 C_D =0.000 A.O.A.=0.0°

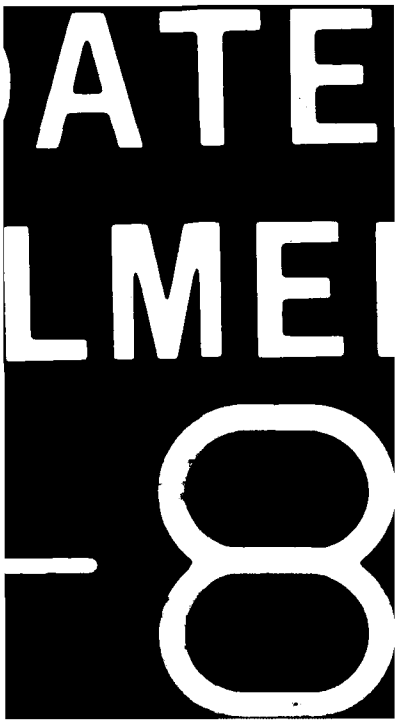
ATE
LME
8